AIMS Mathematics, 11(6): 18715–18745.
DOI: 10.3934/math.2026761
Received: 20 April 2026
Revised: 01 June 2026
Accepted: 10 June 2026
Published: 25 June 2026

https://www.aimspress.com/journal/Math

Research article

Stochastic analysis and ANN-based approximation of measles transmission dynamics under Lévy noise

Anwarud Din*

School of Mechanical and Electrical Engineering, Chengdu University of Technology, Chengdu 610059, China

* **Correspondence:** Email: anwarud@cdut.edu.cn; Tel: +8618520642023.

Abstract: We develop a rigorous mathematical framework for measles transmission that integrates the impact of Lévy noise to account for environmental disturbances. First, the model is formulated, and the uniqueness and existence of a positive solution are investigated. A stochastic threshold is derived to ensure sufficient conditions for the persistence and extinction of the disease. It is demonstrated that the solution curves of the system fluctuate in the neighborhood of the disease-free state of the underlying deterministic model when $\mathbb{R}_D < 1$. We establish sufficient conditions for both extinction and persistence of the disease in the proposed stochastic system. The obtained results demonstrate the ability of the model to characterize the long-term dynamics of measles transmission. Artificial neural networks (ANNs) are employed to approximate the dynamics of the system with Lévy noise. The ANN model, trained on time-series data from stochastic simulations, accurately predicts transitions among the susceptible, exposed, infected, first-dose vaccinated, second-dose vaccinated, and recovered populations. The model's ability to capture stochastic dynamics driven by Lévy noise highlights the potential of ANNs in approximating complex epidemic models. The results validate the theoretical findings and demonstrate that stochastic environmental perturbations can significantly influence the transmission of epidemic diseases. As noise levels increase, a population's ability to sustain the spread of illness is limited, underscoring the critical role of the environment in shaping epidemic dynamics.

Keywords: Lévy noise; artificial neural networks; disease transmission; persistence; noise-induced dynamics
Mathematics Subject Classification: 92D30, 60H10, 60G51, 68T07, 65C30

1. Introduction

In 2018 alone, more than 140,000 deaths worldwide were caused by measles, and included children under five years of age as the primary victims of the disease [1]. Moreover, they demonstrate

that even with active vaccination campaigns, substantial segments of the population in most areas remain vulnerable to measles due to vaccine hesitancy, logistical issues, or insufficient healthcare facilities [2]. These figures indicate that, amongst other social health problems, measles is one of the most threatening infectious diseases worldwide. Various researchers have attempted to extend the findings of the early literature by Anderson and May [3] and Keeling et al. [4] to gain insight into the mysterious processes of measles transmission and potential control strategies. Their within-host and population-level models have provided valuable insights into how measles is transmitted and how best to organis vaccination campaigns. This field has benefited from investigations into numerous mathematical models, both deterministic and stochastic. The main focus of this research is viral transmission within a single-host population, which is often studied in terms of the effects of vaccination and immunity. Grenfell et al. [5] studied the dynamics of measles under various vaccination coverage conditions and confirmed that achieving thresholds of herd immunity is a primary requirement to prevent an outbreak. However, it is not easy to model the Stochastic nature of measles epidemics due to the presence of external variables such as environmental noise and population variation. Exogenous factors can greatly influence the spread and persistence of the disease, especially when vaccine levels fluctuate over time [6]. The role of vaccination in disease prevention and public health has been extensively studied in recent years [7, 8]. Li et al. [9] applied network-based computational techniques to analyse heterogeneous complex diseases.

The mathematical modeling is also a vital instrument to study the epidemiological dynamics of disease spread and come up with effective control measures [10]. The literature has explored a variety of mathematical models to understand measles transmission dynamics, such as compartmental models, which are discussed in the literature by Hethcote [11], and stochastic differential equation models, which are discussed in the literature by Allen [12]. Although deterministic models are more common, stochastic modeling has been significant to the study of the impact of randomness and uncertainty in epidemic dynamics [13–15]. The spread of infectious diseases and the impacts of the diseases can be increased by unpredictable factors such as social dynamics and environmental upheavals. Stochastic models with white noise and jump-diffusion have been especially useful in modeling the effect of a sudden shift in population behavior, vaccine uptake, and environmental dynamics, as well as their interplay, within the context of stochastic models governing population dynamics, stochastic models with white noise and jump-diffusion process have proved especially helpful in modeling the effects of a sharp change in population dynamics, vaccination coverage, and environmental factors and their interaction with each other in the context of stochastic models of population dynamics [16–18]. The latency interval between exposure and development of symptoms in measles is important to take into account because it has a significant effect on the timing of transmission events and control measures. The incubation period usually covers the range of $7 - 21$ days [19]. It has been suggested that Lévy noise can be used as an effective way of modeling abrupt and large-scale changes in population dynamics, including those caused by extreme weather or migration events, in stochastic models [12].

The mathematical modeling of measles transmission dynamics has attracted considerable attention in recent years, with several studies concentrating on diverse geographies and measures for outbreak confinement. One method analyzes the dynamics of measles transmission in Nigeria, employing actual data to explain the disease's propagation and the effects of vaccination initiatives [20]. Similarly, the dynamics of measles transmission have been explored in Pakistan, with a focus on

incorporating real data to improve the accuracy of predictions and inform control measures [21]. Additionally, the seasonal aspects of measles outbreaks have been studied through mathematical models, with particular emphasis on the effects of double-dose vaccination on controlling the spread of the disease [22]. Additional research has concentrated on the analysis and simulation of measles disease dynamics utilizing several control techniques, including vaccination, to assess their efficacy in diminishing transmission [21, 23, 24]. The use of double-dose vaccination in measles models, especially in Bangladesh, has demonstrated potential in stabilizing the illness and avoiding extensive outbreaks [25].

Over the past few years, the artificial intelligence (AI) methods have greatly contributed to the modelling, of complicated infectious disease systems, such as measles, Artificial neural networks (ANNs) have emerged as one of the leading methods among these because of their universal approximation powers and the ability to model nonlinear dynamics as well as flexibility as far as this is concerned [26–28]. ANNs have been successfully applied to synchronization, prediction, and disease-related network analysis in complex systems [29–31]. ANNs are especially useful when one wants to learn the underlying patterns in high-dimensional data without making any explicit assumptions about the structure of the system. This renders ANNs to be a good alternative to the conventional deterministic models, especially when it becomes difficult or impossible to estimate the parameters. Frameworks based on ANN have been effectively utilized in several recent infectious diseases, including HIV, Ebola, COVID-19, and measles where they have been employed to simulate disease progression, predict rates of infections, and estimate the effect of interventions. These models have also shown that they can recreate the temporal behaviour, of epidemiological compartments despite uncertainty. In addition, hybrid methods that combine ANN models with numerical solvers, including the Levenberg-Marquardt (LMB) algorithm, have been found useful in the simulation of compartmental disease models. These hybrid approaches offer low prediction error and high correlation values, which further highlight the increasing importance of machine learning in the field of infectious disease modeling and the adoption of using it as an additional tool to complement mathematical epidemiology methods [32].

This study proposes an SDE system to investigate the dynamic patterns of measles transmission, incorporating the effects of environmental disturbances via Lévy noise. The model categorizes the population into six distinct compartments: susceptible (vulnerable), exposed (latent), infected, first-dose vaccinated, second-dose vaccinated, and recovered/removed individuals. This is especially significant when evaluating the role of vaccination and the influence of stochastic environmental conditions on disease spread. Furthermore, ANNs are employed in the proposed system to simulate the transmission dynamics of measles, while Lévy noise is incorporated to capture environmental fluctuations and random perturbations affecting disease progression. The dynamical behavior of the proposed stochastic model is investigated under the influence of Lévy perturbations. The ANN framework was developed using the LMB algorithm. This approach was selected for its computational efficiency and robustness, particularly in handling the stiffness and nonlinearity of the proposed system.

The key contributions of this study are summarized as follows:

- Development of a compartmental measles transmission model based on a system of nonlinear SDEs, incorporating environmental perturbations through Lévy noise.
- Application of the ANN-LMB methodology to generate high-fidelity numerical approximations

of the model's dynamics, including disease progression and vaccination effects.

- Rigorous comparative analysis of the ANN-LMB approach with traditional deterministic methods, particularly focusing on its predictive accuracy and stability in modeling the impact of Lévy noise on disease dynamics.
- Quantitative validation of the hybrid ANN-LMB modeling framework using various statistical metrics, including mean squared error (MSE), regression diagnostics, and performance similarity indices.

2. Model formulation

The model proposed in [33] examined the dynamical behavior of a deterministic measles transmission model with double-dose vaccination. It also used a physics-informed neural network framework to analyze and predict the temporal evolution of the epidemic system. The model separates the total individuals $\mathbb{N}(t)$ of the community into six classes: vulnerable ($\mathbb{S}$), latent ($\mathbb{E}$), infected ($\mathbb{I}$), people who have taken their first-dose of vaccination ($\mathbb{V}_1$), people who have taken their second-dose of vaccination ($\mathbb{V}_2$), and removed/recovered ($\mathbb{R}$). The dynamics of these groups are captured by a system of ODEs; biologically, the model describes the rate of population change within each compartment.

The susceptible population ($\mathbb{S}(t)$) decreases due to infection and vaccination. Susceptible individuals influence the temporal changes of the population by interacting with infected individuals at a rate determined by the disease transmission rate. Additionally, they may be vaccinated at a specific rate, transitioning to the vaccinated compartments.

The exposed population ($\mathbb{E}(t)$) consists of persons who are exposed to the disease but not yet infected. These individuals transition into the infected class at a rate determined by the flow from the exposed compartment.

The infected population ($\mathbb{I}(t)$) represents individuals who have contracted the disease and can transmit it to others. These individuals may recover at a specific rate or may die due to disease complications. The recovery process is assumed to follow a specific rate, while disease-induced mortality also impacts this class.

The class $\mathbb{V}_1(t)$ represents individuals who have received the first dose of vaccination and therefore possess partial immunity against measles infection. This compartment is formed through the vaccination of susceptible individuals. However, vaccine-induced immunity may gradually wane over time, causing some individuals to return to the susceptible class. In addition, individuals in this compartment may receive a second vaccine dose and transition into the second-dose vaccinated class.

The second-dose vaccinated population $\mathbb{V}_2(t)$ consists of individuals who have received both doses of the vaccine and are assumed to possess stronger and longer-lasting immunity compared with the first-dose vaccinated group. Nevertheless, immunity may still decline over time, allowing some individuals to re-enter the susceptible class due to immunity loss.

The recovered individuals ($\mathbb{R}(t)$) are those who have either recovered from the infection or completed the vaccination process. They may experience natural death over time, which affects the total population.

The population as a whole is influenced by the birth rate, which introduces new vulnerable people into the community. Similarly, the natural death rate applies to all compartments. The total population

remains constant over time, except for changes due to disease-induced mortality and vaccination. The above assumptions for measles transmission are modeled as:

$$\begin{aligned}
\frac{d\mathbb{S}(t)}{dt} &= \Lambda + \omega_v \mathbb{V}_1(t) - \frac{\beta \mathbb{S}(t)\mathbb{I}(t)}{\mathbb{N}(t)} - (\mu + \psi_v)\,\mathbb{S}(t),\\
\frac{d\mathbb{E}(t)}{dt} &= \frac{\beta \mathbb{S}(t)\mathbb{I}(t)}{\mathbb{N}(t)} - (\phi + \mu)\mathbb{E}(t),\\
\frac{d\mathbb{I}(t)}{dt} &= -\left(\gamma + \mu + \phi_1\right)\mathbb{I}(t) + \phi \mathbb{E}(t),\\
\frac{d\mathbb{V}_1(t)}{dt} &= -\left(\mu + \kappa + \omega_v\right)\mathbb{V}_1(t) + \psi_v \mathbb{S}(t),\\
\frac{d\mathbb{V}_2(t)}{dt} &= -(\mu + \omega)\mathbb{V}_2(t) + \kappa \mathbb{V}_1(t),\\
\frac{d\mathbb{R}(t)}{dt} &= -\mu \mathbb{R}(t) + \omega \mathbb{V}_2(t) + \gamma \mathbb{I}(t).
\end{aligned} \tag{2.1}$$

The physical meanings of the parameters are presented in Table 1.

Table 1. Description of parameters used in model (2.1).

Parameter	Description
Λ	New recruitment rate
β	Disease transmission rate
μ	Natural death
ψ_v	Vaccination rate
ω_v	Immunity loss rate from first-dose vaccinated class
ϕ	Transition rate from exposed to infected class
γ	Recovery rate
ϕ_1	Disease-induced death rate
κ	Second-dose vaccination rate
ω	Immunity/recovery rate of second-dose vaccinated individuals

The basic reproduction number of model (2.1) is given by the following expression (for detailed calculations, see [33]).

$$\mathbb{R}_D = \frac{\phi\beta(\omega + \mu)}{(\phi + \mu)(\gamma + \phi_1 + \mu)\left[(\omega_v + \kappa + \mu)(\omega + \mu) + \psi_v(\omega + \mu + \kappa)\right]}.$$

It has been observed that despite incorporating numerous variables and parameters in the model, discrepancies persist between real-world phenomena and the model's predictions. This is particularly evident in epidemic modeling, where environmental factors, such as earthquakes, tsunamis, and weather, can substantially affect disease dynamics. These environmental fluctuations can interrupt the continuity of solutions, and conventional white noise models are inadequate in predicting the system's behavior accurately. Recent studies suggest that integrating Lévy jumps into epidemic models provides a more effective and accurate approach. To control an epidemic and assist in disease

prevention, Lévy noise plays an important role due to its capacity to represent the intrinsic dynamics of infectious diseases [34]. Shah et al. [35] investigated a stochastic hepatitis B epidemic model under Lévy noise with media coverage effects, while Din and Li [36] analyzed the impact of Lévy noise on a stochastic hepatitis B model using real statistical data and a fractal-fractional Atangana–Baleanu framework. Furthermore, El Fatini and Sekkak [37] studied the influence of Lévy noise on a delayed stochastic epidemic model with Crowley–Martin incidence and crowding effects. The deterministic model (2.1) is extended to the following stochastic form:

$$\begin{aligned}
d\mathbb{S}(t) &= \left[\Lambda - \frac{\beta \mathbb{S}(t)\mathbb{I}(t)}{\mathbb{N}(t)} - (\psi_v + \mu)\,\mathbb{S}(t) + \omega_v \mathbb{V}_1(t)\right]dt + \eta_1 \mathbb{S}(t) d\mathbb{W}_1(t) \\
&\quad + \int_{\mathbb{X}} \mathbb{Z}_1(x)\mathbb{S}(t^-)\tilde{N}(dt,dx), \\
d\mathbb{E}(t) &= \left[\frac{\beta \mathbb{S}(t)\mathbb{I}(t)}{\mathbb{N}(t)} - (\mu+\phi)\mathbb{E}(t)\right]dt + \eta_2 \mathbb{E}(t) d\mathbb{W}_2(t) + \int_{\mathbb{X}} \mathbb{Z}_2(x)\mathbb{E}(t^-)\tilde{N}(dt,dx), \\
d\mathbb{I}(t) &= \left[\phi \mathbb{E}(t) - (\mu+\gamma+\phi_1)\,\mathbb{I}(t)\right]dt + \eta_3 \mathbb{I}(t) d\mathbb{W}_3(t) + \int_{\mathbb{X}} \mathbb{Z}_3(x)\mathbb{I}(t^-)\tilde{N}(dt,dx), \\
d\mathbb{V}_1(t) &= \left[\psi_v \mathbb{S}(t) - (\mu+\omega_v+\kappa)\,\mathbb{V}_1(t)\right]dt + \eta_4 \mathbb{V}_1(t) d\mathbb{W}_4(t) + \int_{\mathbb{X}} \mathbb{Z}_4(x)\mathbb{V}_1(t^-)\tilde{N}(dt,dx), \\
d\mathbb{V}_2(t) &= \left[\kappa \mathbb{V}_1(t) - (\mu+\omega)\mathbb{V}_2(t)\right]dt + \eta_5 \mathbb{V}_2(t) d\mathbb{W}_5(t) + \int_{\mathbb{X}} \mathbb{Z}_5(x)\mathbb{V}_2(t^-)\tilde{N}(dt,dx), \\
d\mathbb{R}(t) &= \left[\gamma \mathbb{I}(t) + \omega \mathbb{V}_2(t) - \mu \mathbb{R}(t)\right]dt + \eta_6 \mathbb{R}(t) d\mathbb{W}_6(t) + \int_{\mathbb{X}} \mathbb{Z}_6(x)\mathbb{R}(t^-)\tilde{N}(dt,dx).
\end{aligned} \tag{2.2}$$

The parameters η_i, $i = 1,\ldots,6$ scale the intensities of the Gaussian white-noise terms associated with the Brownian motions $\mathbb{W}_i(t)$, the integral terms $\int_{\mathbb{X}} \mathbb{Z}_i(x)X(t^-)\tilde{N}(dt,dx)$ represent the Lévy jump perturbations, where $\tilde{N} = N(dt,dx) - \nu(dx)dt$ is the compensated Poisson random measure with characteristic measure $\nu(dx)$. The functions $\mathbb{Z}_i(x)$, $i = 1,\ldots,6$ describe the jump amplitudes corresponding to sudden environmental fluctuations and random perturbations affecting the disease transmission dynamics.

3. Global positivity and existence of solutions

A critical biological question arises when examining whether the solution to the stochastic system (2.2), with initial values $(\mathbb{S}(0),\mathbb{E}(0),\mathbb{I}(0),\mathbb{V}_1(0),\mathbb{V}_2(0),\mathbb{R}(0)) \in R^6_+$, remains both global and positive over time. To address this, we begin by defining a set of assumptions and lemmas in the stochastic sense. The time average of a function $\mathbb{Q}(t)$ is defined by

$$\langle \mathbb{Q}(t) \rangle = \frac{1}{t}\int_0^t \mathbb{Q}(x)\,dx.$$

The assumptions $(\mathcal{G}_1)$ and $(\mathcal{G}_2)$ provide the conditions required to establish the existence, uniqueness, and positivity of solutions to system (2.2).

Lemma 3.1. $(\mathcal{G}_1)$ *For every* $\mathbb{M} > 0$*, there exists a constant* $\mathbb{L}_{\mathbb{M}} > 0$ *such that*

$$\int_{\mathbb{Y}} \left|\mathbb{Z}_i(x_1, y) - \mathbb{Z}_i(x_2, y)\right|^2 v(dy) \leq \mathbb{L}_{\mathbb{M}} |x_1 - x_2|^2, \qquad i = 1, \ldots, 6,$$

for

$$|x_1| \vee |x_2| \leq \mathbb{M},$$

where

$$\begin{aligned}
\mathbb{Z}_1(x, y) &= \Omega_1(y)x, \qquad x = \mathbb{S}(t^-),\\
\mathbb{Z}_2(x, y) &= \Omega_2(y)x, \qquad x = \mathbb{E}(t^-),\\
\mathbb{Z}_3(x, y) &= \Omega_3(y)x, \qquad x = \mathbb{I}(t^-),\\
\mathbb{Z}_4(x, y) &= \Omega_4(y)x, \qquad x = \mathbb{V}_1(t^-),\\
\mathbb{Z}_5(x, y) &= \Omega_5(y)x, \qquad x = \mathbb{V}_2(t^-),\\
\mathbb{Z}_6(x, y) &= \Omega_6(y)x, \qquad x = \mathbb{R}(t^-).
\end{aligned}$$

The functions $\Omega_i : \mathbb{Y} \to R, i = 1, \ldots, 6$*, represent the jump amplitudes associated with the Lévy perturbations. Throughout this work, we assume that* $\Omega_i(y) > -1, i = 1, \ldots, 6$*, and* $\int_{\mathbb{Y}} |\Omega_i(y)|^2 v(dy) < \infty, i = 1, \ldots, 6$ *which ensure that the corresponding compensated Poisson integrals are well defined.*

$(\mathcal{G}_2)$ *The function*

$$|\ln(1 + \Omega_i(y))|$$

is bounded, namely,

$$|\ln(1 + \Omega_i(y))| \leq C, \qquad \Omega_i(y) > -1,$$

where C is a positive constant.

Theorem 3.1. *For any initial value* $(\mathbb{S}(0), \mathbb{E}(0), \mathbb{I}(0), \mathbb{V}_1(0), \mathbb{V}_2(0), \mathbb{R}(0)) \in \mathbb{R}^6_+$*, system* (2.2) *admits a unique global solution* $(\mathbb{S}(t), \mathbb{E}(t), \mathbb{I}(t), \mathbb{V}_1(t), \mathbb{V}_2(t), \mathbb{R}(t)), t \geq 0$*. Moreover, the solution remains positive almost surely, that is,* $(\mathbb{S}(t), \mathbb{E}(t), \mathbb{I}(t), \mathbb{V}_1(t), \mathbb{V}_2(t), \mathbb{R}(t)) \in \mathbb{R}^6_+, t \geq 0, \quad a.s.$

Proof. $(\mathcal{G}_1)$ and the drift and the diffusion are locally Lipschitz. Hence, by the standard existence and pathwise uniqueness result, for each $(\mathbb{S}(0), \mathbb{E}(0), \mathbb{I}(0), \mathbb{V}_1(0), \mathbb{V}_2(0), \mathbb{R}(0)) \in R^6_+$, there exists a unique maximal (local) solution defined on an interval $t \in [0, \tau_e)$, where τ_e denotes the explosion time. It remains to prove that the solution does not explode, that is, $\tau_e = \infty$ almost surely. Choose $m_0 \geq 1$ large enough so that each initial component lies in the interval $\left[\frac{1}{m_0}, m_0\right]$. For every integer $m \geq m_0$, introduce the stopping time

$$\begin{aligned}
\tau_m = \inf \Bigg\{ & t \in [0, \tau_e) : \min\Big(\mathbb{S}(t), \mathbb{E}(t), \mathbb{I}(t), \mathbb{V}_1(t), \mathbb{V}_2(t), \mathbb{R}(t)\Big) \leq \frac{1}{m} \\
& \text{or} \max\Big(\mathbb{S}(t), \mathbb{E}(t), \mathbb{I}(t), \mathbb{V}_1(t), \mathbb{V}_2(t), \mathbb{R}(t)\Big) \geq m \Bigg\}.
\end{aligned} \tag{3.1}$$

By construction, $\{\tau_m\}_{m \geq m_0}$ is nondecreasing in m. Define

$$\tau_\infty := \lim_{m \to \infty} \tau_m,$$

so that $\tau_\infty \leq \tau_e$. To complete the argument, it is enough to show that $\tau_\infty = \infty$ almost surely. Suppose, to the contrary, that this fails. Then there exist constants $T > 0$ and $\varepsilon \in (0, 1)$ such that

$$\mathbb{P}\Big(\tau_\infty \leq T\Big) > \varepsilon.$$

Consequently, there exists an integer $m_1 \geq m_0$ such that

$$P\{\tau_m \leq T\} \geq \epsilon \quad \text{for} \quad m \geq m_1.$$

To proceed further, let us consider a C^2-function $V : R_+^6 \to R_+$by

$$\begin{aligned}\mathbb{G}(\mathbb{S}, \mathbb{E}, \mathbb{I}, \mathbb{V}_1, \mathbb{V}_2, \mathbb{R}) = (-\ln \mathbb{S} + \mathbb{S} - 1) + (-\ln \mathbb{E} + \mathbb{E} - 1) + (-\ln \mathbb{I} + \mathbb{I} - 1) \\ + (-\ln \mathbb{V}_1 + \mathbb{V}_1 - 1) + (-\ln \mathbb{V}_2 + \mathbb{V}_2 - 1) + (\mathbb{R} - \ln \mathbb{R} - 1).\end{aligned} \tag{3.2}$$

Applying Itô's formula to (3.2) and let, $d\zeta = (dt, dx)$, we obtain

$$\begin{aligned}L\mathbb{G} = LVdt + \eta_1(\mathbb{S} - 1)d\mathbb{W}_1(t) + \eta_2(\mathbb{E} - 1)d\mathbb{W}_2(t) + \eta_3(\mathbb{I} - 1)d\mathbb{W}_3(t) \\ + \eta_4(\mathbb{V}_1 - 1)d\mathbb{W}_4(t) + \eta_5(\mathbb{V}_2 - 1)d\mathbb{W}_5(t) + \eta_5(\mathbb{R} - 1)d\mathbb{W}_6(t) \\ + \int_{\mathbb{X}}[\mathbb{Z}_1(x)\mathbb{S} - \ln(1 + \mathbb{Z}_1(x))]\tilde{\mathbb{N}}(d\zeta) + \int_{\mathbb{X}}[\mathbb{Z}_2(x)\mathbb{E} - \ln(1 + \mathbb{Z}_2(x))]\tilde{\mathbb{N}}(d\zeta) \\ + \int_{\mathbb{X}}[\mathbb{Z}_3(x)\mathbb{I} - \ln(1 + \mathbb{Z}_3(x))]\tilde{\mathbb{N}}(d\zeta) + \int_{\mathbb{X}}[\mathbb{Z}_4(x)\mathbb{V}_1 - \ln(1 + \mathbb{Z}_4(x))]\tilde{\mathbb{N}}(d\zeta) \\ + \int_{\mathbb{X}}[\mathbb{Z}_5(x)\mathbb{V}_2 - \ln(1 + \mathbb{Z}_5(x))]\tilde{\mathbb{N}}(d\zeta) + \int_{\mathbb{X}}[\mathbb{Z}_6(x)\mathbb{R} - \ln(1 + \mathbb{Z}_6(x))]\tilde{\mathbb{N}}(d\zeta).\end{aligned} \tag{3.3}$$

Where,

$$\begin{aligned}L\mathbb{G} = \left(1 - \frac{1}{\mathbb{S}}\right)\left(\Lambda - \frac{\beta\mathbb{S}(t)\mathbb{I}(t)}{\mathbb{N}(t)} - (\psi_v + \mu)\,\mathbb{S}(t) + \omega_v\mathbb{V}_1(t)\right) \\ + \frac{\eta_1^2}{2} + \int_{\mathbb{X}}[\mathbb{Z}_1(x) - \ln(\mathbb{Z}_1(x) + 1)]v(dx) \\ + \left(1 - \frac{1}{\mathbb{E}}\right)\left(\frac{\beta\mathbb{S}(t)\mathbb{I}(t)}{\mathbb{N}(t)} - (\mu + \phi)\mathbb{E}(t)\right) + \frac{\alpha_2^2}{2} + \int_{\mathbb{X}}[\mathbb{Z}_2(x) - \ln(\mathbb{Z}_2(x) + 1)]v(dx) \\ + \left(1 - \frac{1}{\mathbb{I}}\right)\left(\phi\mathbb{E}(t) - (\mu + \gamma + \phi_1)\,\mathbb{I}(t)\right) + \frac{\eta_3^2}{2} + \int_{\mathbb{X}}[\mathbb{Z}_3(x) - \ln(1 + \mathbb{Z}_3(x))]v(dx) \\ + \left(1 - \frac{1}{\mathbb{V}_1}\right)\left(\psi_v\mathbb{S}(t) - (\mu + \omega_v + \kappa)\,\mathbb{V}_1(t)\right) + \frac{\eta_4^2}{2} + \int_{\mathbb{X}}[\mathbb{Z}_4(x) - \ln(1 + \mathbb{Z}_4(x))]v(dx) \\ + \left(1 - \frac{1}{\mathbb{V}_2}\right)\left(\kappa\mathbb{V}_1(t) - (\mu + \omega)\mathbb{V}_2(t)\right) + \frac{\eta_5^2}{2} + \int_{\mathbb{X}}[\mathbb{Z}_5(x) - \ln(1 + \mathbb{Z}_5(x))]v(dx) \\ + \left(1 - \frac{1}{\mathbb{R}}\right)\left(\gamma\mathbb{I}(t) + \omega\mathbb{V}_2(t) - \mu\mathbb{R}(t)\right) + \frac{\eta_6^2}{2} + \int_{\mathbb{X}}[\mathbb{Z}_6(x) - \ln(1 + \mathbb{Z}_6(x))]v(dx).\end{aligned} \tag{3.4}$$

$$\begin{aligned}L\mathbb{G} \leq \Lambda + \beta + \psi_v + 6\mu + \phi + \gamma + \phi_1 + \omega_v + \kappa + \omega \\ + \sum_{i=1}^{6}\frac{\eta_i^2}{2} + \sum_{i=1}^{6}\int_{\mathbb{X}}[\mathbb{Z}_i(x) - \ln(1 + \mathbb{Z}_i(x))]\,v(dx) = \mathbb{K}.\end{aligned} \tag{3.5}$$

By integrating both sides of relation (3.3) throughout the interval 0 to $\tau_\rho \wedge T$ and subsequently computing the expectation, we derive

$$\begin{aligned} 0 \leq & E\Big[\mathbb{G}(\mathbb{S}(\tau_\rho \wedge T), \mathbb{E}(\tau_\rho \wedge T), \mathbb{I}(\tau_\rho \wedge T), \mathbb{V}_1(\tau_\rho \wedge T), \mathbb{V}_2(\tau_\rho \wedge T), \mathbb{R}(\tau_\rho \wedge T))\Big] \\ & \leq \mathbb{G}(\mathbb{S}_0, \mathbb{E}_0, \mathbb{I}_0, \mathbb{V}_{1,0}, \mathbb{V}_{2,0}, \mathbb{R}_0) + E\Big[\int_0^{\tau_\rho \wedge T} \mathbb{K}, dt\Big] \\ & \leq \mathbb{G}(\mathbb{S}_0, \mathbb{E}_0, \mathbb{I}_0, \mathbb{V}_{1,0}, \mathbb{V}_{2,0}, \mathbb{R}_0) + T\mathbb{K}. \end{aligned} \tag{3.6}$$

We get $P(\Omega_\rho) \geq \epsilon$ for $\rho_1 \leq \rho$ by taking $\Omega_\rho = \{T \geq \tau_\rho\}$. There is at least one component of $(\mathbb{S}(\tau_\rho, \omega), \mathbb{E}(\tau_\rho, \omega), \mathbb{I}(\tau_\rho, \omega), \mathbb{V}_1(\tau_\rho, \omega), \mathbb{V}_2(\tau_\rho, \omega), \mathbb{R}(\tau_\rho, \omega))$ equal to $\frac{1}{\rho}$ or ρ for all $\omega \in \Omega_\rho$. Since at least one component of

$$(\mathbb{S}_{\tau_\rho}, \mathbb{E}_{\tau_\rho}, \mathbb{I}_{\tau_\rho}, \mathbb{V}_{1,\tau_\rho}, \mathbb{V}_{2,\tau_\rho}, \mathbb{R}_{\tau_\rho})$$

is equal to either ρ or $1/\rho$, we have

$$\mathbb{G}(\mathbb{S}_{\tau_\rho}, \mathbb{E}_{\tau_\rho}, \mathbb{I}_{\tau_\rho}, \mathbb{V}_{1,\tau_\rho}, \mathbb{V}_{2,\tau_\rho}, \mathbb{R}_{\tau_\rho}) \geq (\rho - 1 - \ln\rho) \wedge \left(\frac{1}{\rho} - 1 + \ln\rho\right).$$

Thus,

$$\mathbb{G}(\mathbb{S}_{\tau_\rho}, \mathbb{E}_{\tau_\rho}, \mathbb{I}_{\tau_\rho}, \mathbb{V}_{1,\tau_\rho}, \mathbb{V}_{2,\tau_\rho}, \mathbb{R}_{\tau_\rho}) \geq (\rho - 1 - \ln\rho) \wedge \left(\frac{1}{\rho} - 1 + \ln\rho\right). \tag{3.7}$$

By $P(\tau_\rho \leq T) \geq \epsilon$ and Eq (3.6), we obtain

$$\begin{aligned} \mathbb{G}(\mathbb{S}_0, \mathbb{E}_0, \mathbb{I}_0, \mathbb{V}_{1,0}, \mathbb{V}_{2,0}, \mathbb{R}_0) + T\mathbb{K} &\geq \mathbb{E}\left[\mathbf{1}_{\Omega_\rho}\mathbb{G}(\mathbb{S}_{\tau_\rho}, \mathbb{E}_{\tau_\rho}, \mathbb{I}_{\tau_\rho}, \mathbb{V}_{1,\tau_\rho}, \mathbb{V}_{2,\tau_\rho}, \mathbb{R}_{\tau_\rho})\right] \\ &\geq \epsilon\left[(\rho - 1 - \ln\rho) \wedge \left(\frac{1}{\rho} - 1 + \ln\rho\right)\right]. \end{aligned} \tag{3.8}$$

Here, $\mathbf{1}_{\Omega_\rho}$ denotes the indicator function of the event Ω_ρ. Letting $\rho \to \infty$ in (3.8) leads to the contradiction

$$\infty > \mathbb{G}(\mathbb{S}_0, \mathbb{E}_0, \mathbb{I}_0, \mathbb{V}_{1,0}, \mathbb{V}_{2,0}, \mathbb{R}_0) + T\mathbb{K} = \infty.$$

Therefore, the assumption is false, and hence $\tau_\infty = \infty$ almost surely. This completes the proof. □

4. The extinction of the model

Lemma 4.1. *If model (2.2), $(\mathbb{S}, \mathbb{E}, \mathbb{I}, \mathbb{V}_1, \mathbb{V}_2, \mathbb{R})$, is a root with starting approximation $(\mathbb{S}_0, \mathbb{E}_0, \mathbb{I}_0, \mathbb{V}_{1,0}, \mathbb{V}_{2,0}, \mathbb{R}_0) \in R_+^6$, then a.s.*

$$\lim_{t\to\infty} \frac{\mathbb{S}(t) + \mathbb{E}(t) + \mathbb{I}_1(t) + \mathbb{V}_1(t) + \mathbb{V}_2(t) + \mathbb{R}(t)}{t} = 0. \tag{4.1}$$

Further,

$$\lim_{t\to\infty} \frac{1}{t}\int_0^t \mathbb{S}(r)\, d\mathbb{X}_1(r) = 0, \quad \lim_{t\to\infty} \frac{1}{t}\int_0^t \mathbb{E}(r)\, d\mathbb{X}_2(r) = 0, \quad \lim_{t\to\infty} \frac{1}{t}\int_0^t \mathbb{I}(r)\, d\mathbb{X}_3(r) = 0,$$

$$\lim_{t\to\infty} \frac{1}{t}\int_0^t \mathbb{V}_1(r)\, d\mathbb{X}_4(r) = 0, \quad \lim_{t\to\infty} \frac{1}{t}\int_0^t \mathbb{V}_2(r)\, d\mathbb{X}_5(r) = 0, \quad \lim_{t\to\infty} \frac{1}{t}\int_0^t \mathbb{R}(r)\, d\mathbb{X}_5(r) = 0.$$

Proof. The explanation of the preceding claim is skipped here, since the concluding remarks may be reached using the technique described in the development of Lemma (4.1) in Zhang et al. [38]. □

Theorem 4.1. *If* $\mathbf{R}_0 < 1$*, then the infection dies out exponentially almost surely, i.e.,*

$$\begin{aligned}
\limsup_{t\to\infty} \mathbb{S}(t) &\leq \frac{\omega_v\psi_v + \Lambda[(\psi_v+\mu)(\mu+\omega_v+\phi_1) - \psi_v\omega_v]}{((\psi_v+\mu)(\mu+\omega_v+\phi_1))^2},\\
\limsup_{t\to\infty} \mathbb{E}(t) &\leq 0,\\
\limsup_{t\to\infty} \mathbb{I}(t) &\leq 0,\\
\limsup_{t\to\infty} \mathbb{V}_1(t) &\leq \frac{\psi_v\Lambda}{(\psi_v+\mu)(\mu+\omega_v+\phi_1)(\psi_v\omega_v)},\\
\limsup_{t\to\infty} \mathbb{V}_2(t) &\leq \frac{\kappa\psi_v\Lambda}{(\mu+\omega)(\psi_v+\mu)(\mu+\omega_v+\phi_1)(\psi_v\omega_v)},\\
\limsup_{t\to\infty} \mathbb{R}(t) &\leq \frac{\omega\kappa\psi_v\Lambda}{\mu(\mu+\omega)(\psi_v+\mu)(\mu+\omega_v+\phi_1)(\psi_v\omega_v)}, a.s.
\end{aligned}$$

Proof. We know that

$$\begin{aligned}
\frac{\mathbb{E}(t)-\mathbb{E}(0)}{t} &= \frac{\beta_1\langle \mathbb{S}\rangle\langle \mathbb{I}\rangle}{\langle \mathbb{N}\rangle} - (\mu+\phi)\langle \mathbb{E}\rangle + \frac{\eta_2}{t}\int_0^t \mathbb{E}(r)d\mathbb{W}_2(r)\\
&\quad + \frac{1}{t}\int_0^t\left[\int_{\mathbb{X}} \mathbb{Z}_2(x)\mathbb{E}(t^-)\tilde{\mathbb{N}}(d\zeta)\right]dr,\\
\frac{\mathbb{I}(t)-\mathbb{I}(0)}{t} &= \phi\langle \mathbb{E}\rangle - (\mu+\gamma+\phi_1)\langle \mathbb{I}\rangle + \frac{\eta_3}{t}\int_0^t \mathbb{I}(r)d\mathbb{W}_3(r)\\
&\quad + \frac{1}{t}\int_0^t\left[\int_{\mathbb{X}} \mathbb{Z}_3(x)\mathbb{I}(t^-)\tilde{\mathbb{N}}(d\zeta)\right]dr.
\end{aligned} \tag{4.2}$$

Let,

$$P(t) = \frac{\mathbb{E}(t)-\mathbb{E}(0)}{t} + \frac{\mathbb{I}(t)-\mathbb{I}(0)}{t}.$$

So we get

$$\begin{aligned}
P(t) &= \frac{\beta\langle \mathbb{S}\rangle\langle \mathbb{I}\rangle}{\langle \mathbb{N}\rangle} - (\mu+\phi)\langle \mathbb{E}\rangle + \phi\langle \mathbb{E}\rangle - (\mu+\gamma+\phi_1)\langle \mathbb{I}\rangle\\
&\quad + \frac{\eta_2}{t}\int_0^t \mathbb{E}(r)d\mathbb{W}_2(r) + \frac{\eta_3}{t}\int_0^t \mathbb{I}(r)d\mathbb{W}_3(r)\\
&\quad + \frac{1}{t}\int_0^t\left[\int_{\mathbb{X}} \mathbb{Z}_2(x)\mathbb{E}(t^-)\tilde{\mathbb{N}}(d\zeta)\right]dr + \frac{1}{t}\int_0^t\left[\int_{\mathbb{X}} \mathbb{Z}_3(x)\mathbb{I}(t^-)\tilde{\mathbb{N}}(d\zeta)\right]dr.
\end{aligned}$$

Applying Itô's formula to $P(t)$, let $H = \ln P(t)$,

$$\begin{aligned}
d\ln P(t) &= L\mathbb{H}dt + \eta_2 d\mathbb{W}_2(t) + \eta_3 d\mathbb{W}_3(t) + \int_{\mathbb{X}}\Big[\ln(1+\mathbb{Z}_2(x))\Big]\tilde{\mathbb{N}}(d\zeta)\\
&\quad + \int_{\mathbb{X}}\Big[\ln(1+\mathbb{Z}_3(x))\Big]\tilde{\mathbb{N}}(d\zeta),
\end{aligned}$$

where,

$$L\mathbb{H} = \left[\frac{\beta\mathbb{S}}{\mathbb{N}} - (\mu+\gamma+\phi_1) - \frac{\eta_2^2+\eta_3^2}{2}\right]dt - \int_{\mathbb{X}}\left[\mathbb{Z}_2(x) - \ln(1+Z_2(x)\right]vdx$$
$$- \int_{\mathbb{X}}\left[\mathbb{Z}_3(x) - \ln(1+Z_3(x)\right]vdx.$$

Applying Itô's formula to $d\ln P(t)$, we have

$$\begin{aligned}\frac{\ln P(t) - \ln P(0)}{t} &= \frac{\beta\langle\mathbb{S}\rangle}{\langle\mathbb{N}\rangle} - (\mu+\gamma+\phi_1) - \frac{\eta_2^2-\eta_3^2}{2} - \int_{\mathbb{X}}\left[\mathbb{Z}_2(x) - \ln(1+\mathbb{Z}_2(x)\right]vdx\\ &\quad - \int_{\mathbb{X}}\left[\mathbb{Z}_3(x) - \ln(1+\mathbb{Z}_3(x)\right]vdx + \frac{\eta_2}{t}\int_0^t d\mathbb{W}_2(x) + \frac{\eta_3}{t}\int_0^t d\mathbb{W}_3(x)\\ &\quad + \frac{1}{t}\int_{\mathbb{X}}[\ln(1+\mathbb{Z}_2(x))]\tilde{\mathbb{N}}(d\zeta) + \frac{1}{t}\int_{\mathbb{X}}[\ln(1+\mathbb{Z}_3(x))]\tilde{\mathbb{N}}(d\zeta),\\ &\le \beta - (\mu+\gamma+\phi_1) - \frac{\eta_2^2-\eta_3^2}{2} - \int_{\mathbb{X}}\left[\mathbb{Z}_2(x) - \ln(1+\mathbb{Z}_2(x)\right]vdx\\ &\quad - \int_{\mathbb{X}}\left[\mathbb{Z}_3(x) - \ln(1+\mathbb{Z}_3(x)\right]vdx + \frac{\eta_2}{t}\int_0^t d\mathbb{W}_2(x) + \frac{\eta_3}{t}\int_0^t d\mathbb{W}_3(x)\\ &\quad + \frac{1}{t}\int_{\mathbb{X}}[\ln(1+\mathbb{Z}_2(x))]\tilde{\mathbb{N}}(d\zeta) + \frac{1}{t}\int_{\mathbb{X}}[\ln(1+\mathbb{Z}_3(x))]\tilde{\mathbb{N}}(d\zeta).\end{aligned}$$

$$\begin{aligned}\text{Let } M(t) &= \frac{\eta_2}{t}\int_0^t d\mathbb{W}_2(x) + \frac{\eta_3}{t}\int_0^t d\mathbb{W}_3(x) + \frac{1}{t}\int_{\mathbb{X}}[\ln(1+\mathbb{Z}_2(x))]\tilde{\mathbb{N}}(d\zeta)\\ &\quad + \frac{1}{t}\int_{\mathbb{X}}[\ln(1+\mathbb{Z}_3(x))]\tilde{\mathbb{N}}(d\zeta),\end{aligned}$$

which is called the local continuous-martingale if $M(0) = 0$ and similarly $X(0) = 0$.

$$\lim_{t\to\infty}\sup\frac{M(t)}{t} = 0, \quad \text{and} \quad \lim_{t\to\infty}\sup\frac{X(t)}{t} = 0.$$

Then,

$$\begin{aligned}\lim_{t\to\infty}\sup\frac{\ln P(t)}{t} &\le \left[\mu+\gamma+\phi_1 + \frac{\eta_2^2-\eta_3^2}{2} + \int_{\mathbb{X}}\left[\mathbb{Z}_2(x) - \ln(1+\mathbb{Z}_2(x)\right]vdx\right.\\ &\quad \left. + \int_{\mathbb{X}}\left[\mathbb{Z}_3(x) - \ln(1+\mathbb{Z}_3(x)\right]vdx\right](\mathbf{R}_0 - 1),\end{aligned} \tag{4.3}$$

where,

$$\mathbf{R}_0 = \frac{\beta}{\mu+\gamma+\phi_1 + \frac{\eta_2^2-\eta_3^2}{2} + \int_{\mathcal{X}}[Z_2(x) - \ln(1+Z_2(x))]\,v(dx) + \int_{\mathcal{X}}[Z_3(x) - \ln(1+Z_3(x))]\,v(dx)}.$$

If $\mathbf{R}_0 < 1$, then

$$\lim_{t\to\infty}\left\langle\mathbb{I}(t)\right\rangle = 0, \quad \text{a.s.}$$

We may now readily derive the following equations,

$$\lim_{t\to\infty}\left\langle \mathbb{E}(t)\right\rangle = 0,$$

$$\lim_{t\to\infty}\left\langle \mathbb{S}(t)\right\rangle = \frac{\omega_v\psi_v + \Lambda[(\psi_v+\mu)(\mu+\omega_v+\phi_1)-\psi_v\omega_v]}{((\psi_v+\mu)(\mu+\omega_v+\phi_1))^2},$$

$$\lim_{t\to\infty}\left\langle \mathbb{V}_1(t)\right\rangle = \frac{\psi_v\Lambda}{(\psi_v+\mu)(\mu+\omega_v+\phi_1)(\psi_v\omega_v)},$$

$$\lim_{t\to\infty}\left\langle \mathbb{V}_2(t)\right\rangle = \frac{\kappa\psi_v\Lambda}{(\mu+\omega)(\psi_v+\mu)(\mu+\omega_v+\phi_1)(\psi_v\omega_v)},$$

$$\lim_{t\to\infty}\left\langle \mathbb{R}(t)\right\rangle = \frac{\omega\kappa\psi_v\Lambda}{\mu(\mu+\omega)(\psi_v+\mu)(\mu+\omega_v+\phi_1)(\psi_v\omega_v)}.$$

Thus, we completed our proof of Theorem 4.1. □

5. The persistence of the model

This section explores the long-term effects of the condition by focusing on its temporal persistence. To establish a solid theoretical framework, we first define persistence in an averaged sense. This definition follows Din et al. [36]. The concept will serve as a foundation for understanding the condition's enduring impacts and potential long-term consequences.

Lemma 5.1. ***(Strong law) [36]:*** *Consider a continuous function $F = \{F_t\}_{0\le t}$ that exists as a local martingale. If at $t \to 0$, the function tends to zero, then:*

$$\lim_{t\to\infty}\langle F,F\rangle_t = \infty, \quad a.s. \quad \Rightarrow \quad \lim_{t\to\infty}\frac{F_t}{\langle F,F\rangle_t} = 0, \quad a.s.$$

$$\lim_{t\to\infty}\sup\frac{\langle F,F\rangle_t}{t} < 0, \quad a.s. \quad \Rightarrow \quad \lim_{t\to\infty}\frac{F_t}{t} = 0, \quad a.s.$$

Lemma 5.2. *Let $h \in C([0,\infty)\times\Omega,(0,\infty))$ and $\mathcal{H} \in C([0,\infty)\times\Omega,R)$. Assume that*

$$\lim_{t\to\infty}\frac{\mathcal{H}(t)}{t} = 0, \quad a.s.,$$

and that, for every $t \ge 0$,

$$\ln h(t) \;\ge\; \xi_0\, t \;-\; \xi\int_0^t h(s)\,ds \;+\; \mathcal{H}(t), \quad a.s.$$

Then the time average of h satisfies

$$\liminf_{t\to\infty}\langle h(t)\rangle \;\ge\; \frac{\Xi_0}{\Xi}, \quad a.s.,$$

where $\Xi, \Xi_0 \in R$, $\Xi > 0$, and $\Xi_0 \ge 0$; see [36, 37].

To study persistence in mean for system (2.2), we next state the main result of this section as a theorem.

Theorem 5.1. *If* $\mathbf{R}_0^s > 1$*, then for any initial approximation* $(\mathbb{S}(0), \mathbb{E}(0), \mathbb{I}(0), \mathbb{V}_1(0), \mathbb{V}_2(0), \mathbb{R}(0)) \in R_+^6$*, the epidemic* $\mathbb{I}(t)$ *follows an axiom. If the following holds:*

$$\liminf_{t\to\infty}\langle \mathbb{I}(t)\rangle \geq \frac{3\Lambda\left[\sqrt[3]{\mathbf{R}_0^s}-1\right]}{C_1\beta}, \quad a.s.,$$

where

$$C_1 = \frac{\Lambda}{\left(\psi_v+\mu+\frac{\eta_1^2}{2}+\int_{\mathcal{X}}\left[\mathbb{Z}_1(x)-\ln(1+\mathbb{Z}_1(x))\right]v(dx)\right)}.$$

Consequently we can assert that the disease will persist throughout the community. We define:

$$\mathbf{R}_0^s = \frac{\beta\Lambda\phi}{a_1b_1c_1},$$

where

$$a = \left(\psi_v+\mu+\frac{\eta_1^2}{2}+\mathcal{J}_1\right), b = \left(\mu+\phi+\frac{\eta_2^2}{2}+\mathcal{J}_2\right), c = \left(\mu+\gamma+\phi_1+\frac{\eta_3^2}{2}+\mathcal{J}_3\right),$$

and $\mathcal{J}_i = \int_{\mathcal{X}}\left[\mathbb{Z}_i(x)-\ln(1+\mathbb{Z}_i(x))\right]v(dx)$ *for* $i = 1, 2, 3.$

Proof. Set

$$\mathbb{H} = -C_1\ln\mathbb{S} - C_2\ln\mathbb{E} - C_3\ln\mathbb{I}. \tag{5.1}$$

Applying, Itô's formula

$$\begin{aligned} d\mathbb{H} = &-\frac{C_1\Lambda}{\mathbb{S}} + C_1\beta\mathbb{I} + C_1(\psi_v+\mu) - \frac{C_1\omega_v\mathbb{V}_1}{\mathbb{S}} + \frac{C_1\eta_1^2}{2} + C_1\mathcal{J}_1 - \frac{C_2\beta\mathbb{S}\mathbb{I}}{\mathbb{N}} \\ &- C_2(\mu+\phi) + \frac{C_2\eta_2^2}{2} + C_2\mathcal{J}_2 - \frac{C_3\phi\mathbb{E}}{\mathbb{I}} + C_3(\mu+\gamma+\gamma) + \frac{C_3\eta_3^2}{2} + C_3\mathcal{J}_3, \end{aligned}$$

so

$$\begin{aligned} d\mathbb{H} \leq &\left(-\frac{C_1\lambda}{\mathbb{S}} - \frac{C_2\beta\mathbb{S}\mathbb{I}}{\mathbb{N}} - \frac{C_3\phi\mathbb{E}}{\mathbb{I}}\right) + C_1\left(\psi_v+\mu+\frac{\eta_1^2}{2}+\mathcal{J}_1\right) \\ &+ C_2\left(\mu+\phi+\frac{\eta_2^2}{2}+\mathcal{J}_2\right) + C_3\left(\mu+\gamma+\phi_1+\frac{\eta_3^2}{2}+\mathcal{J}_3\right) + \frac{C_1\beta\mathbb{I}}{\mathbb{N}}. \end{aligned}$$

Then

$$\begin{aligned} d\mathbb{H} \leq &-3\sqrt[3]{C_1C_2C_3\beta\phi\Lambda} + C_1\left(\psi_v+\mu+\frac{\eta_1^2}{2}+\mathcal{J}_1\right) \\ &+ C_2\left(\mu+\phi+\frac{\eta_2^2}{2}+\mathcal{J}_2\right) + C_3\left(\mu+\gamma+\gamma)+\frac{\eta_3^2}{2}+\mathcal{J}_3\right) + C_1\beta\mathbb{I}. \end{aligned} \tag{5.2}$$

Let

$$C_1 = \frac{\Lambda}{\left(\psi_v + \mu + \frac{\eta_1^2}{2} + \mathcal{J}_1\right)},\ C_2 = \frac{\Lambda}{\left(\mu + \phi + \frac{\eta_2^2}{2} + \mathcal{J}_2\right)},\ C_3 = \frac{\Lambda}{\left(\mu + \gamma + \gamma + \frac{\eta_3^2}{2} + \mathcal{J}_3\right)}.$$

Consider,

$$a = \left(\psi_v + \mu + \frac{\eta_1^2}{2} + \mathcal{J}_1\right), b = \left(\mu + \phi + \frac{\eta_2^2}{2} + \mathcal{J}_2\right), c = \left(\mu + \gamma + \gamma + \frac{\eta_3^2}{2} + \mathcal{J}_3\right).$$

Then we get

$$\begin{aligned} L\mathbb{H} &\leq -3\sqrt[3]{\frac{\Lambda^3\beta\Lambda\phi}{abc}} + 3\Lambda + C_1\beta\mathbb{I}, \\ &\leq -3\Lambda\left[\sqrt[3]{\frac{\beta\Lambda\phi}{abc}} - 1\right] + C_1\beta\mathbb{I}, \\ &\leq -3\Lambda\left[\sqrt[3]{\mathbb{R}_0^s} - 1\right] + C_1\beta\mathbb{I}. \end{aligned} \tag{5.3}$$

Letting Eq (5.3) in Eq (5.1) and using the values of $\mathcal{J}_i$, then taking integral on both sides we have

$$\begin{aligned} &\frac{\mathbb{H}(\mathbb{S}(t),\mathbb{E}(t),\mathbb{I}(t)) - \mathbb{H}(\mathbb{S}(0),\mathbb{E}(0),\mathbb{I}(0))}{t} \leq -3\Lambda\left[\sqrt[3]{\mathbf{R}_0^s} - 1\right] + C_1\beta\mathbb{I} - \frac{C_1\eta_1^2\mathbb{W}_1(t)}{t} \\ &- \frac{C_2\eta_2^2\mathbb{W}_2(t)}{t} - \frac{C_3\eta_3^2\mathbb{W}_3(t)}{t} - C_1\int_{\mathbb{X}}[\mathbb{Z}_1(x)\mathbb{S} - \ln(1+\mathbb{Z}_1(x))]\tilde{\mathbb{N}}(d\zeta) \\ &- C_2\int_{\mathbb{X}}[\mathbb{Z}_2(x)\mathbb{E} - \ln(1+\mathbb{Z}_2(x))]\tilde{\mathbb{N}}(d\zeta) - C_3\int_{\mathbb{X}}[\mathbb{Z}_3(x)\mathbb{I} - \ln(1+\mathbb{Z}_3(x))]\tilde{\mathbb{N}}(d\zeta), \\ &\leq -3\Lambda\left[\sqrt[3]{\mathbf{R}_0^s} - 1\right] + C_1\beta\mathbb{I} + \Psi(t), \end{aligned} \tag{5.4}$$

where,

$$\begin{aligned} \Psi(t) = &-\frac{C_1\eta_1^2}{t}\mathbb{W}_1(t) - \frac{C_2\eta_2^2}{t}\mathbb{W}_2(t) - \frac{C_3\eta_3^2}{t}\mathbb{W}_3(t) - C_1\int_{\mathcal{X}}\left[\mathbb{Z}_1(x)\mathbb{S} - \ln\left(1+\mathbb{Z}_1(x)\right)\right]\widetilde{\mathbb{N}}(d\zeta) \\ &- C_2\int_{\mathcal{X}}\left[\mathbb{Z}_2(x)\mathbb{E} - \ln\left(1+\mathbb{Z}_2(x)\right)\right]\widetilde{\mathbb{N}}(d\zeta) - C_3\int_{\mathcal{X}}\left[\mathbb{Z}_3(x)\mathbb{I} - \ln\left(1+\mathbb{Z}_3(x)\right)\right]\widetilde{\mathbb{N}}(d\zeta). \end{aligned}$$

By the strong law given in Lemma 5.1, it follows that

$$\lim_{t\to\infty}\Psi(t) = 0.$$

Moreover, from (5.4), we obtain

$$C_1\beta\langle\mathbb{I}\rangle \geq 3\Lambda\left(\sqrt[3]{\mathbb{R}_0^s} - 1\right) - \Psi(t) + \frac{G(\mathbb{S}(t),\mathbb{E}(t),\mathbb{I}(t)) - G(\mathbb{S}(0),\mathbb{E}(0),\mathbb{I}(0))}{t}. \tag{5.5}$$

Combining Lemma 5.2 with (5.5) and using $\Psi(t) \to 0$ as $t \to \infty$, we deduce that

$$\liminf_{t\to\infty}\langle \mathbb{I}(t)\rangle \geq \frac{3\Lambda\left[\sqrt[3]{\mathbf{R}_0^s}-1\right]}{C_1\beta}, \quad \text{a.s.}$$

In particular, the time-average of $\mathbb{I}(t)$ is bounded away from zero whenever $\mathbb{R}_0^s > 1$. This completes the proof of Theorem 5.1. □

6. Numerical analysis

This section serves two main purposes: first, to develop a numerical scheme to approximate the solution of model (2.2); and second, to explore instructive examples that illustrate how different parameters influence the system's dynamics. By achieving these objectives, we aim to deepen our understanding of the model's behavior and examine how the system's dynamics are affected by various variables and parameters.

6.1. Milstein scheme with Lévy jumps

In the case of model (2.2), we make use of the proven numerical method presented in [39], which has been utilized in a variety of research works, such as in [40–42]. We will assume the following in our numerical scheme, namely: x^* is represented as a member of the set $\mathbb{S}$, $\mathbb{N}^*$, is represented as a member of the natural numbers $\mathbb{N}$, n is a number (an integer) that changes in the range 0 and $\mathbb{N}^*$ and finally, the time step, denoted by Δt, is a division of T by $\mathbb{N}^*$. The population size at time step n is given by the equation $\mathbb{N}^n = \mathbb{S}^n + \mathbb{E}^n + \mathbb{I}^n + \mathbb{V}_1^n + \mathbb{V}_2^n + \mathbb{R}^n$. To compute the increments of the Brownian motion in time, they multiply the increments by the independent statistics of standard normal variables of values of the increments and the square root of the time change which is denoted as the increments of the Brownian motion or in other words, the maxims of the probability distribution of the Brownian motion of the particle are the square root of the increments of the probability distribution of the motion of the particle. Further, the Poisson increment is given as $\Delta\mathbb{L}_n$, which is a Poisson distribution of intensity v, over which X is an interval of 0 to infinity with the intensity function $v(X)$ being taken as 1. Keeping these components, the Milstein numerical scheme of the model (2.2) is formulated as follows:

$$\begin{aligned}
\mathbb{S}^{n+1} &= \mathbb{S}^n + \left[\Lambda - \frac{\beta\mathbb{S}^n\mathbb{I}^n}{\mathbb{N}^n} - (\psi_v+\mu)\mathbb{S}^n + \omega_v\mathbb{V}_1^n\right]\Delta t + \eta_1\mathbb{S}^n\Delta\mathbb{W}_{1,n} + \frac{\eta_1^2}{2}\mathbb{S}^n(\Delta\mathbb{W}_{1,n}^2 - \Delta t)\\
&\quad + \mathbb{Z}_1(x^*)\mathbb{S}^n\Delta\mathbb{L}n,\\
\mathbb{E}^{n+1} &= \mathbb{E}^n + \left[\frac{\beta\mathbb{S}^n\mathbb{I}^n}{\mathbb{N}^n} - (\mu+\phi)\mathbb{E}^n\right]\Delta t + \eta_2\mathbb{E}^n\Delta\mathbb{W}_{2,n}\\
&\quad + \frac{\eta_2^2}{2}\mathbb{E}^n(\Delta\mathbb{W}_{2,n}^2 - \Delta t) + \mathbb{Z}_2(x^*)\mathbb{E}^n\Delta\mathbb{L}n,\\
\mathbb{I}^{n+1} &= \mathbb{I}^n + \left[\phi\mathbb{E}^n - (\mu+\gamma+\phi_1)\mathbb{I}^n - \frac{\beta\mathbb{S}^n\mathbb{I}^n}{\mathbb{N}^n}\right]\Delta t + \eta_3\mathbb{I}^n\Delta\mathbb{W}_{3,n} + \frac{\eta_3^2}{2}\mathbb{I}^n(\Delta\mathbb{W}_{3,n}^2 - \Delta t)\\
&\quad + \mathbb{Z}_3(x^*)\mathbb{I}^n\Delta\mathbb{L}n,
\end{aligned}$$

$$\mathbb{V}_1^{n+1} = \mathbb{V}_1^n + \left[\psi_v \mathbb{S}^n - (\mu + \omega_v + \kappa)\mathbb{V}_1^n\right]\Delta t + \eta_4 \mathbb{V}_1^n \Delta \mathbb{W}_{4,n} + \frac{\eta_4^2}{2}\mathbb{V}_1^n(\Delta \mathbb{W}_{4,n}^2 - \Delta t) + \mathbb{Z}_4(x^*)\mathbb{V}_1^n \Delta \mathbb{L}n,$$

$$\mathbb{V}_2^{n+1} = \mathbb{V}_2^n + \left[\kappa \mathbb{V}_1^n - (\mu + \omega)\mathbb{V}_2^n\right]\Delta t + \eta_5 \mathbb{V}_2^n \Delta \mathbb{W}_{5,n} + \frac{\eta_5^2}{2}\mathbb{V}_2^n(\Delta \mathbb{W}_{5,n}^2 - \Delta t) + \mathbb{Z}_5(x^*)\mathbb{V}_2^n \Delta \mathbb{L}n,$$

$$\mathbb{R}^{n+1} = \mathbb{R}^n + \left[\gamma \mathbb{I}^n + \omega \mathbb{V}_2^n - \mu \mathbb{R}^n\right]\Delta t + \eta_6 \mathbb{R}^n \Delta \mathbb{W}_{6,n} + \frac{\eta_6^2}{2}\mathbb{R}^n(\Delta \mathbb{W}_{6,n}^2 - \Delta t) + \mathbb{Z}_6(x^*)\mathbb{R}^n \Delta \mathbb{L}_n.$$

It is just one of the possible numerical techniques that can be used in solving the model. Another approach is the so-called piecewise polynomial technique for exact model, which has been demonstrated to be useful for addressing complex systems, as noted in the source cited in [43]. Past studies have confirmed the usefulness of the PPTEM method for simulating complex models, as demonstrated in the works of [40–42] and others.

6.2. Numerical simulation of extinction

To support the analytical results obtained for models (2.2) and (2.1), particularly Theorem 4.1, the system is discretized with a time increment of $\Delta t = 0.10$ and prescribed initial data. For model (2.2), the parameter configuration is chosen as $\Lambda = 0.5, \beta = 0.01, \psi_v = 0.03, \mu = 0.10, \omega_v = 0.12, \phi = 0.23, \phi_1 = 0.12, \gamma = 0.01, \kappa = 0.34, \omega = 0.23$, and the noise intensity parameters are taken as $\eta_1 = 1.45, \eta_2 = 0.44, \eta_3 = 0.12, \eta_4 = 1.90, \eta_5 = 1.06, \eta_6 = 0.70$, with step-related coefficients $h_1 = 0.02, h_2 = 0.06, h_3 = 0.004, h_4 = 0.04$. To examine the prediction stated in Theorem 4.1, we evaluate the threshold value $\mathbf{R}_0$. In the considered parameter regime, $\mathbf{R}_0 < 1$, this condition leads to the gradual elimination of the infection, and the prevalence of the disease converges to zero as $t \to \infty$. Shown in Figure 1, which depicts the progression of the disease over time. measles therapy is effective among patients, but it might not be effective in the same individuals or may vary over time. To explain this variability, we assume Lévy noise in the model. Lévy noise refers to random fluctuations in a stochastic system that may be caused by multiple external sources. Using Lévy noise, we can visualize the uncertainty in the disease dynamics. Specifically, increasing the level of noise in these models can significantly affect the system, potentially accelerating the elimination of infected compartments. The disease behavior and response to treatment are greatly affected by such changes because of the external environmental factors that cause such fluctuations.

6.3. Numerical simulation of persistence

In this section, we validate the results of Theorem 5.1, consdring, the parameter values and initial conditions are $\Lambda = 1.5, \beta = 0.05, \psi_v = 0.50, \mu = 0.15, \omega_v = 0.25, \phi = 0.45, \phi_1 = 0.50, \gamma = 0.05, \kappa = 0.45, \omega = 0.25$, and the noise intensities, $\eta_1 = 2.00, \eta_2 = 1.5, \eta_3 = 0.50, \eta_4 = 2.5, \eta_5 = 2.50, \eta_6 = 1.50$, with $h_1 = 0.02, h_2 = 0.06, h_3 = 0.004, h_4 = 0.04$. Based on the selected parameters, we find that the threshold value, $\mathbf{R}_0^s > 1$. According to Theorem 5.1, this confirms that the infectious disease, as described by the model (2.2), will persist in the population. The condition $\mathbf{R}_0^s > 1$ ensures the ongoing spread of the disease, and this is visually confirmed in Figure 2. The model also demonstrates that, with minimal noise, the disease persists when $\mathbf{R}_0^s > 1$. As

shown in Figures 2a–2f, the system's trajectories approach stable equilibrium values, indicating stochastic asymptotic stability. These results align with the predictions of Theorem 5.1. Further, as the intensity of the white noise increases over time, Figure 2 shows that viral cell proliferation intensifies, leading to continuous persistence of the measles infection in the population. This results in a stable, well-defined dynamic pattern, confirming that the infection persists when white noise is sufficiently loud.

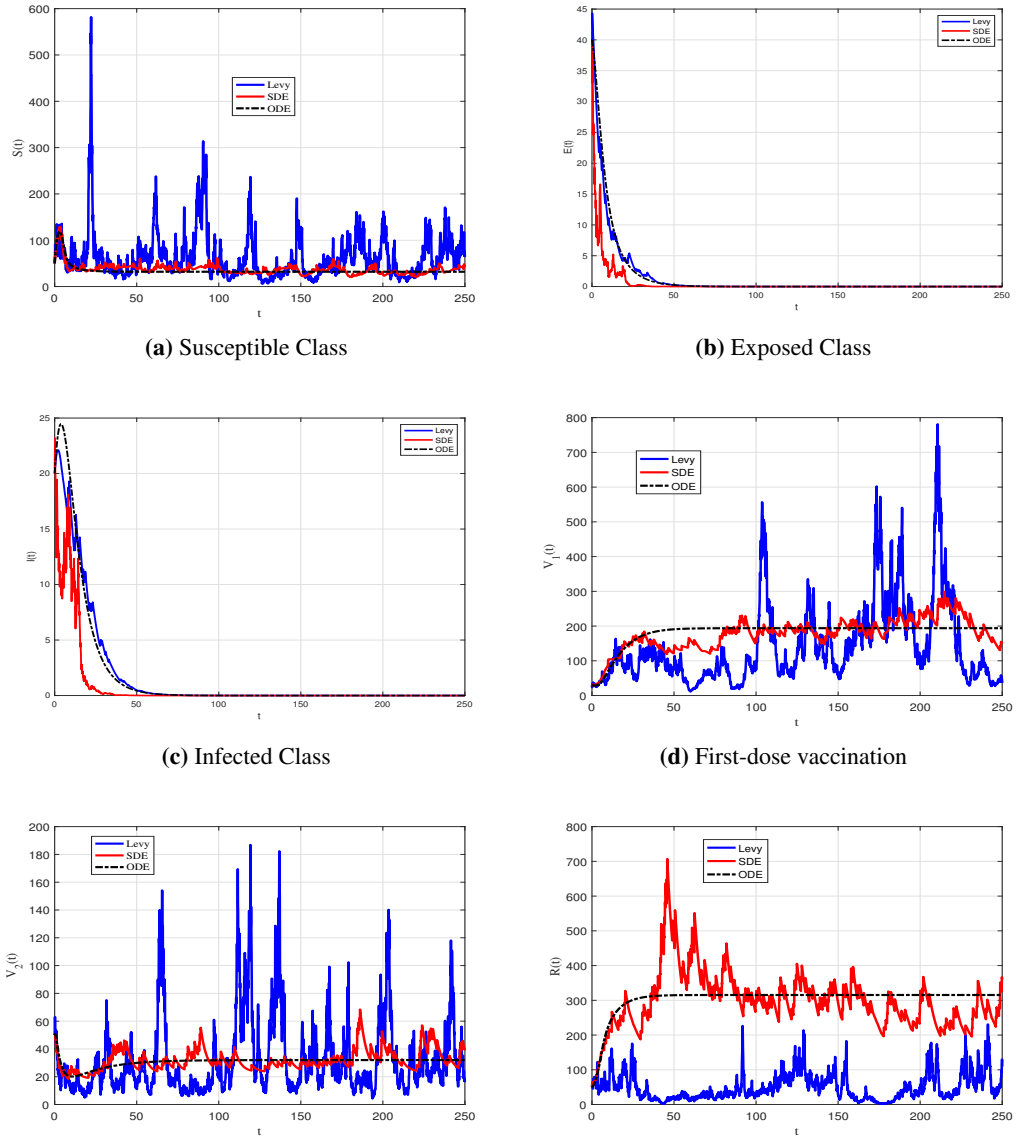

(a) Susceptible Class

(b) Exposed Class

(c) Infected Class

(d) First-dose vaccination

(e) Second-dose vaccination

(f) Recovered Class

Figure 1. Temporal evolution of different compartments in the model (2.2), showing the solution paths for the susceptible, exposed, infected, vaccinated (first and second doses), and recovered classes.

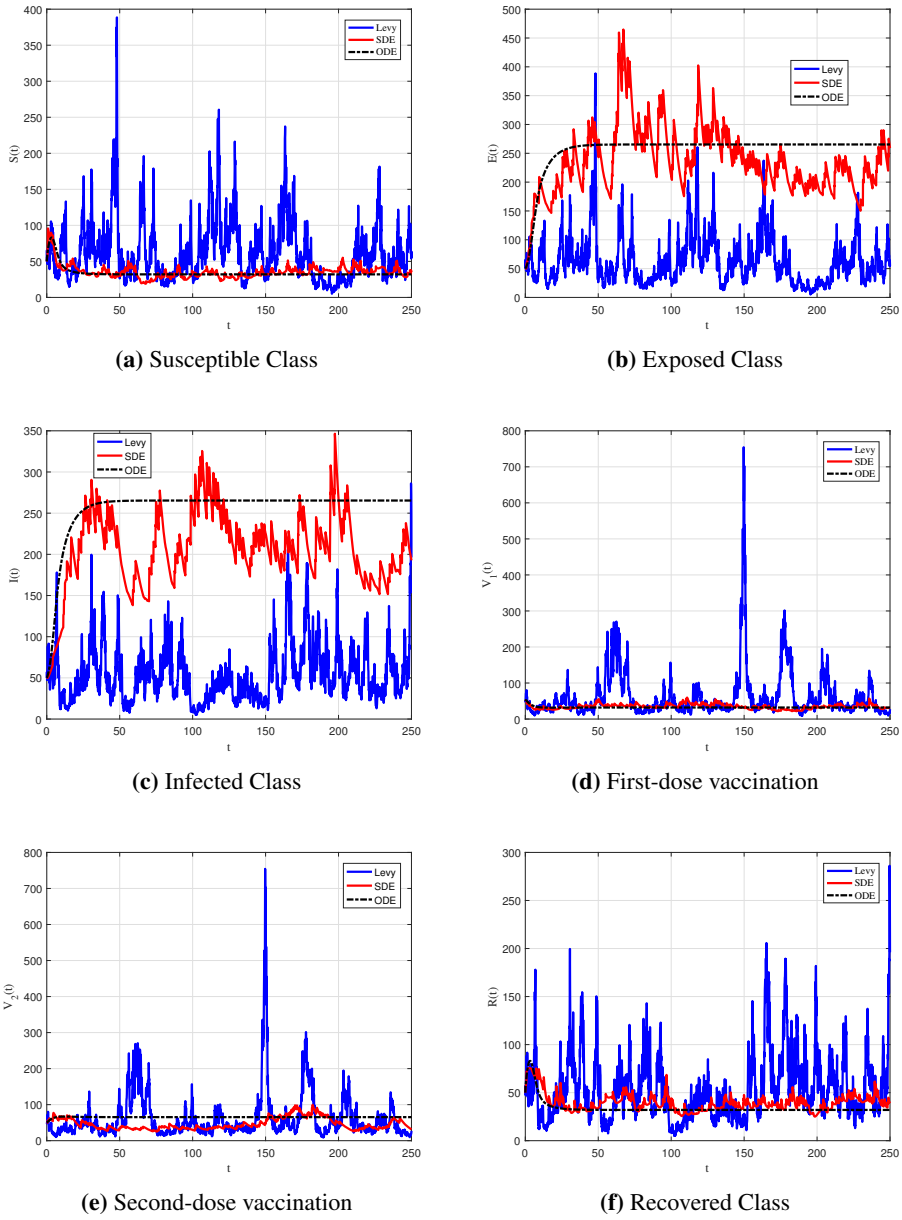

(a) Susceptible Class **(b)** Exposed Class

(c) Infected Class **(d)** First-dose vaccination

(e) Second-dose vaccination **(f)** Recovered Class

Figure 2. Solution trajectories of model (2.2) for the susceptible (S), exposed (E), infected (I), first-dose vaccinated (V_1), second-dose vaccinated (V_2), and recovered (R) populations.

6.4. Effects of Lévy noise

Now we analyze the impact of Lévy noise on the system dynamics using numerical simulations. We focus on the sensitivity of the threshold value $\mathbf{R}_0^s$ and examine how changes in its value influence the long-term behavior of the model. At this point, we will shift to the discussion of the long-term consequences of the system. To increase the realism of the model, two forms of noise are added as in the model (2.2). To support this method, we need to consider the impact that the Lévy noise and the white noise make on model dynamics. In this analysis, we chose various values of the noise intensities, namely, $\eta_1, \eta_2, \eta_3, \eta_4, \eta_5, \eta_6$, so that they are not too small, and the rest of the parameter values were

the same as those in Figure 2. We further changed the values of $h_1 = 0.6$, $h_2 = 0.75$, $h_3 = 0.44$, and $h_4 = 0.33$ to such large values that we could see their effect on the dynamics of the model. The findings show that under these selected parameters, model (2.2) causes the silence of the disease in the population, and the deterministic version of the model has a sustained epidemic. This observation indicates that Lévy noise plays a major part in the process of pushing the system to the extinction of the disease. Moreover, Figure 3 illustrates these trajectories and shows how stochastic variability contributes to the disease dynamics.

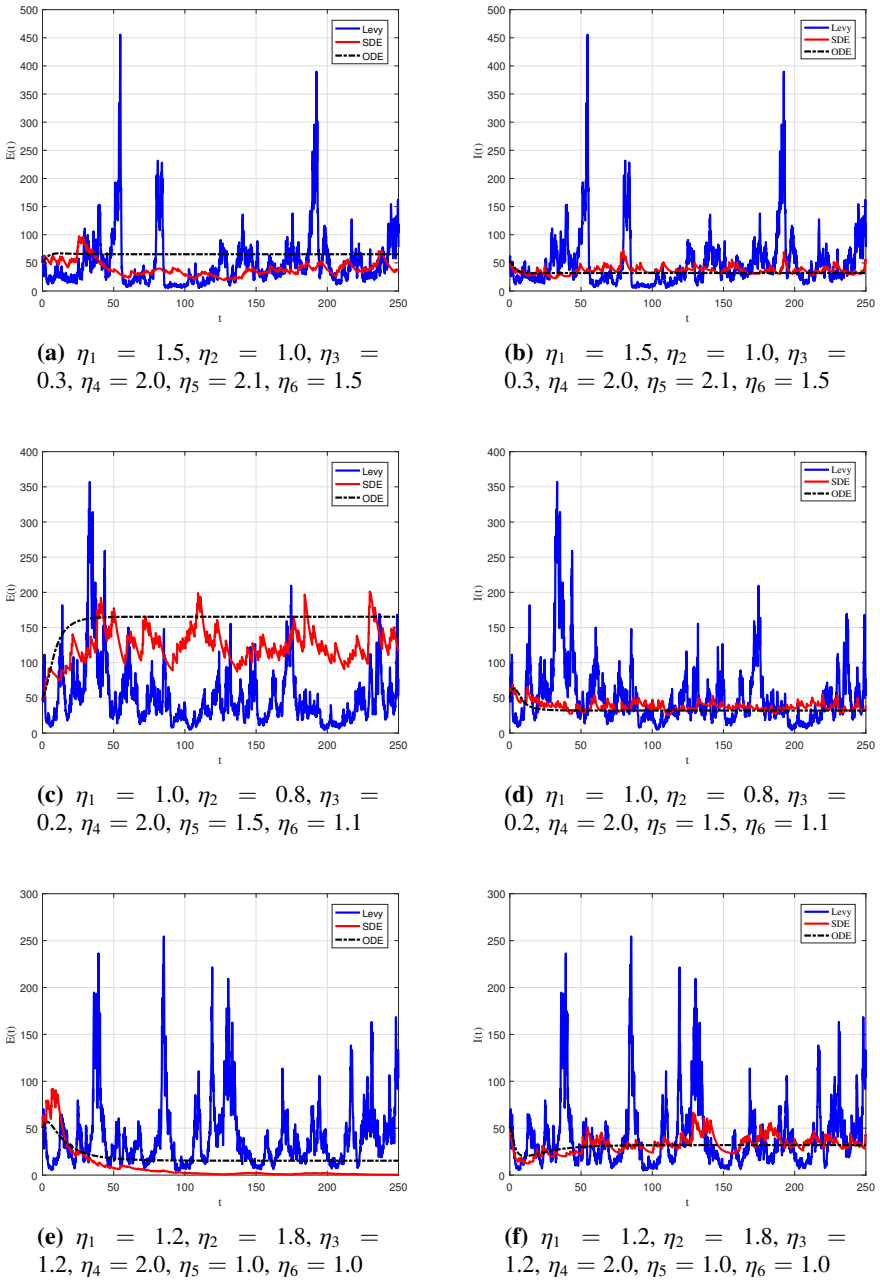

(a) $\eta_1 = 1.5$, $\eta_2 = 1.0$, $\eta_3 = 0.3$, $\eta_4 = 2.0$, $\eta_5 = 2.1$, $\eta_6 = 1.5$

(b) $\eta_1 = 1.5$, $\eta_2 = 1.0$, $\eta_3 = 0.3$, $\eta_4 = 2.0$, $\eta_5 = 2.1$, $\eta_6 = 1.5$

(c) $\eta_1 = 1.0$, $\eta_2 = 0.8$, $\eta_3 = 0.2$, $\eta_4 = 2.0$, $\eta_5 = 1.5$, $\eta_6 = 1.1$

(d) $\eta_1 = 1.0$, $\eta_2 = 0.8$, $\eta_3 = 0.2$, $\eta_4 = 2.0$, $\eta_5 = 1.5$, $\eta_6 = 1.1$

(e) $\eta_1 = 1.2$, $\eta_2 = 1.8$, $\eta_3 = 1.2$, $\eta_4 = 2.0$, $\eta_5 = 1.0$, $\eta_6 = 1.0$

(f) $\eta_1 = 1.2$, $\eta_2 = 1.8$, $\eta_3 = 1.2$, $\eta_4 = 2.0$, $\eta_5 = 1.0$, $\eta_6 = 1.0$

Figure 3. The effects of Lévy noise on the solution trajectories of the infected $\mathbb{I}(t)$ and exposed $\mathbb{E}(t)$ compartments.

7. Training and error evaluation using the artificial neural network

This section presents the ANN training procedure, performance measures, and error analysis used to assess the predictive capability of the proposed framework.

7.1. Euler–Maruyama discretization

The stochastic trajectories used for ANN training were generated using the Euler–Maruyama discretization with step size $\Delta t = 0.1$. The resulting dataset was subsequently employed for training, validation, and testing of the ANN-LMB framework. The Euler–Maruyama scheme is employed only to generate the stochastic dataset required for ANN training, whereas the Milstein scheme is used in the stochastic simulations presented in the previous section. The corresponding update rules for each state variable are given by

$$\begin{aligned}
\mathbb{S}_{n+1} &= \max\left[\mathbb{S}_n + \left(\Lambda - \frac{\beta \mathbb{S}_n \mathbb{I}_n}{N_n} - (\psi_v + \mu)\,\mathbb{S}_n + \omega_v \mathbb{V}_{1,n}\right)\Delta t + \eta_1 \mathbb{S}_n \sqrt{\Delta t}\,\xi_1 \right.\\
&\qquad \left. + \int_{\mathbb{X}} \mathbb{Z}_1(x)\mathbb{S}_{n^-}\tilde{\mathbb{N}}(d\zeta), 0\right],\\
\mathbb{E}_{n+1} &= \max\left[\mathbb{E}_n + \left(\frac{\beta \mathbb{S}_n \mathbb{I}_n}{N_n} - (\mu + \phi)\mathbb{E}_n\right)\Delta t + \eta_2 \mathbb{E}_n \sqrt{\Delta t}\,\xi_2 + \int_{\mathbb{X}} \mathbb{Z}_2(x)\mathbb{E}_{n^-}\tilde{\mathbb{N}}(d\zeta), 0\right],\\
\mathbb{I}_{n+1} &= \max\left[\mathbb{I}_n + (\phi \mathbb{E}_n - (\mu + \gamma + \phi_1)\,\mathbb{I}_n)\,\Delta t + \eta_3 \mathbb{I}_n \sqrt{\Delta t}\,\xi_3 + \int_{\mathbb{X}} \mathbb{Z}_3(x)\mathbb{I}_{n^-}\tilde{\mathbb{N}}(d\zeta), 0\right],\\
\mathbb{V}_{1,n+1} &= \max\left[\mathbb{V}_{1,n} + (\psi_v \mathbb{S}_n - (\mu + \omega_v + \kappa)\,\mathbb{V}_{1,n})\,\Delta t + \eta_4 \mathbb{V}_{1,n} \sqrt{\Delta t}\,\xi_4 \right.\\
&\qquad \left. + \int_{\mathbb{X}} \mathbb{Z}_4(x)\mathbb{V}_{1,n^-}\tilde{\mathbb{N}}(d\zeta), 0\right],\\
\mathbb{V}_{2,n+1} &= \max\left[\mathbb{V}_{2,n} + (\kappa \mathbb{V}_{1,n} - (\mu + \omega)\mathbb{V}_{2,n})\,\Delta t + \eta_5 \mathbb{V}_{2,n} \sqrt{\Delta t}\,\xi_5 + \int_{\mathbb{X}} \mathbb{Z}_5(x)\mathbb{V}_{2,n^-}\tilde{\mathbb{N}}(d\zeta), 0\right],\\
\mathbb{R}_{n+1} &= \max\left[\mathbb{R}_n + (\gamma \mathbb{I}_n + \omega \mathbb{V}_{2,n} - \mu \mathbb{R}_n)\,\Delta t + \eta_6 \mathbb{R}_n \sqrt{\Delta t}\,\xi_6 + \int_{\mathbb{X}} \mathbb{Z}_6(x)\mathbb{R}_{n^-}\tilde{\mathbb{N}}(d\zeta), 0\right],
\end{aligned}$$

where $\xi_i \sim \mathcal{N}(0,1)$, $i = 1, \ldots, 6$ are independent standard normal random variables representing the Brownian motion increments. Furthermore, the terms containing $\tilde{\mathbb{N}}(d\zeta)$ account for the jump component generated by the underlying Lévy process.

7.2. Artificial neural network approximation

To obtain a data-driven surrogate for the system dynamics, we build separate feedforward neural networks, each dedicated to one state variable. The networks are trained using the time grid $\{t_n\}_{n=1}^{N}$ together with the simulated state snapshots $\left[(\mathbb{S}_n, \mathbb{E}_n, \mathbb{I}_n, \mathbb{V}_{1,n}, \mathbb{V}_{2,n}, \mathbb{R}_n)\right]_{n=1}^{N}$.

Input vector. For each time index n, the input feature vector is defined by

$$\mathbf{u}_n = \left[t_n, \mathbb{S}_n, \mathbb{E}_n, \mathbb{I}_n, \mathbb{V}_{1,n}, \mathbb{V}_{2,n}, \mathbb{R}_n \right]^\top \in \mathbb{R}^7.$$

Network outputs (targets). Let $\mathcal{N}_\mathbb{S}, \mathcal{N}_\mathbb{E}, \mathcal{N}_\mathbb{I}, \mathcal{N}_{V_1}, \mathcal{N}_{V_2}, \mathcal{N}_\mathbb{R}$ denote the six regressors. They produce the approximations

$$\hat{\mathbb{S}}_n = \mathcal{N}_\mathbb{S}(\mathbf{u}_n), \hat{\mathbb{E}}_n = \mathcal{N}_\mathbb{E}(\mathbf{u}_n), \hat{\mathbb{I}}_n = \mathcal{N}_\mathbb{I}(\mathbf{u}_n),$$
$$\hat{\mathbb{V}}_{1,n} = \mathcal{N}_{V_1}(\mathbf{u}_n), \hat{\mathbb{V}}_{2,n} = \mathcal{N}_{V_2}(\mathbf{u}_n), \hat{\mathbb{R}}_n = \mathcal{N}_\mathbb{R}(\mathbf{u}_n).$$

Model structure and training. Each regressor is implemented as a shallow (single-hidden-layer) feedforward network. Training is performed with the Levenberg–Marquardt optimization routine (Matlab `trainlm`), and the hidden layer contains 10 neurons.

Loss function. Parameter estimation is carried out by minimizing the empirical mean squared error between the network outputs and the simulated targets:

$$\mathrm{MSE} = \frac{1}{N} \sum_{n=1}^{N} \left(y_n - \hat{y}_n \right)^2,$$

where y_n denotes the corresponding simulated value for the variable being learned.

7.3. Evaluation metrics

To ensure a comprehensive evaluation, we assess predictive performance using standard regression diagnostics along with visual checks.

(1) Mean Squared Error (MSE). The MSE measures the average squared discrepancy between predictions and reference values:

$$\mathrm{MSE} = \frac{1}{N} \sum_{i=1}^{N} \left(y_i - \hat{y}_i \right)^2.$$

Smaller values indicate closer agreement with the simulated trajectories.

(2) Coefficient of Determination ($\mathbf{R}^2$). To quantify explained variance, we report

$$\mathbf{R}^2 = 1 - \frac{\sum_{i=1}^{N} (y_i - \hat{y}_i)^2}{\sum_{i=1}^{N} (y_i - \bar{y})^2},$$

where $\bar{y} = \frac{1}{N} \sum_{i=1}^{N} y_i$. Values of $\mathbf{R}$ closer to 1 indicate better fit, while negative values can occur when the predictor performs worse than the mean baseline.

(3) Error distribution. Prediction errors are computed as $e_i = y_i - \hat{y}_i$, and their histogram is used to summarize bias (shift from zero) and dispersion across the dataset.

(4) Trajectory comparison. Finally, we overlay $\hat{y}(t)$ and $y(t)$ over time to visually inspect how well the learned model follows the reference dynamics. Residual plots $e(t)$ versus time are also included to reveal persistent patterns or systematic deviations.

Interpretation: Large values of $\mathbf{R}^2$ (near one) and low values of MSE and symmetric error histograms show a well trained ANN that can accurately represent the stochastic model results. This is the section where you will be able to find the numeric representation of your measles model, its ANN integration. Approximating the behavior of the system is performed with the help of the Euler-Maruyama discretization technique and ANN training. The evaluation metrics are such that the trained ANNs can predict with precision the system dynamics including the effects of Lévy process..

8. ANN simulation results

In the ANN simulations, we utilized normalized initial conditions for all state variables in the model. This normalization ensured that the inputs were normalized to a constant range of values, enabling the network to converge faster during training and enhancing its stability. In particular, all the initial values of the state variables, $\mathbb{S}(t)$, $\mathbb{E}(t)$, $\mathbb{I}(t)$, $\mathbb{V}_1(t)$, $\mathbb{V}_2(t)$, and $\mathbb{R}(t)$, were rescaled to the range of 0 to 1. This initial preprocessing is important to training neural networks because it avoids gradient explosion or vanishing gradients, which typically occur when training a deep network with large or divergent numerical values. The normalized initial conditions also help the ANN generalize better, thereby making model predictions more certain at various stages of the simulation. The figures that present the results include: 4–7.

To evaluate the predictive capability of the proposed ANN framework, the generated stochastic simulation dataset was divided into three subsets: 70% for training, 15% for validation, and 15% for testing. The test dataset was not used during training. This partition enables evaluation of network performance on previously unseen stochastic trajectories and helps assess the ANN model's generalization capability. The ANN simulation results provide a robust comparison between the ANN predictions and the SDE model with Lévy noise for the dynamics of the $S(t)$, $E(t)$, $I(t)$, $V_1(t)$, $V_2(t)$, and $R(t)$ classes. The following discusses the performance of the model for each class based on the results presented in Figure 4. In subfigure 4a, we find the comparison of the SDE model (with Lévy jumps) and the ANN predictions of the Susceptible class. The model is able to describe the changes in the susceptible population, and the sharp peaks denote stochastic transitions that are caused by Lévy noise. The error plot under the trajectory indicates that the results of the ANN are very close to the SDE model, with a small deviation. The small oscillations of transitions are well forecasted, which proves the ability of the ANN to cope with stochastic processes with Lévy jumps. In the case of the $E(t)$, group in subfigure 4b of the SDE model, the population growth is characteristic, and then a rapid decay occurs. The ANN is quite close to the above trend in that it also achieves the initial sharp peak and subsequent stabilization of the exposed population. The error plot shows that the ANN is doing very well and all the errors are zero or at most very small, particularly at the stages when the $E(t)$, class becomes steady. The Lévy jumps make minor changes, and the model represents them sufficiently. In subfigure 4c, the Infected class has a peak and a sharp drop. Irregular peaks of the stochasticization of the dynamics of infection are reflected by the SDE model, whereas the ANN predictions closely trace the overall trend. It is shown in the error plot that the ANN shows a close approximation to the behaviour of the infected population with few speculations during the early and

late transitions. In the case of the first-dose vaccinated population in subfigure 4d, the SDE model produces the oscillating trends associated with the dynamics of vaccinations when exposed to Lévy jumps. The ANN represents the overall oscillating behaviour, having a few deviations. The error plot validates the fact that the ANN works well in estimating the dynamics of the vaccination process, particularly in the large fluctuations when the population is growing. In the subfigure displaying 4f, a gradual increase with fewer fluctuations is observed in the second-dose vaccinated category. The SDE model is able to explain these oscillations due to Lévy noise, and the ANN is not left behind. The error plot indicates that there are a few differences between the ANN and the SDE model, which indicates that the model is reliable for predicting the effect of vaccination and is stochastic in nature. Lastly, 4f subfigure illustrates an upward trend of the Recovered class as a result of the process of recovery. The SDE model has Lévy jumps, which make the population have fluctuations in the recovery path. These changes are well represented by the ANN as depicted in the error plot. Despite minor variations in the initial recovery phase, the ANN is a strong predictor, which indicates its capability to duplicate the overall trend of recovery as affected by the Lévy noise. The values of the variables and parameters are taken from Figure 2.

The findings of the ANN simulation on the $E(t)$ and $I(t)$ classes (shown in Figure 5), together with the error values, give a holistic view of the model performance in the dynamics of the system with Lévy noise. The error histogram of the Exposed class presented in Figure 5a shows that the number of mistakes concentrated around the zero point is significant, and all the training, validation, and test sets have many instances of very small prediction error. This implies that the ANN model has been well generalized to the training data and has good performance on unknown validation and test data. Nevertheless, some cases with larger errors can still be observed, especially during transition phases, which is likely caused by the complicated nature of Lévy jumps influencing the population dynamics at such critical points. In Figure 5c, the mean squared error (MSE) plot confirms that the model's validation performance improved steadily over epochs, with the best validation performance reaching an exceptionally low value of 7.8549×10^{-9} at epoch 284. The fact that the MSE for the training, validation, and test sets converge suggests that the model is not overfitting and can reliably predict across various stages of the dynamics. Figure 5b shows that the gradient, mu, and validation checks fluctuate but converge, confirming that the training process is stable and that the model improves incrementally over epochs. The output vs. target plots in Figure 5d for the Infected class further illustrate that the ANN predictions are highly accurate, as evidenced by the high $\mathbf{R}^2$ values (close to 1 for training, validation, and test sets). The ANN's ability to closely match the SDE model predictions for both the $E(t)$ and $I(t)$ classes, especially given the inherent randomness introduced by Lévy jumps, demonstrates the power of neural networks in approximating complex stochastic systems. While small deviations remain, particularly during rapid transitions or high-fluctuation regimes, the overall performance is highly commendable. The small prediction error indicates that the ANN effectively captures the system dynamics. Table 2 shows that the proposed ANN-LMB framework achieves lower prediction errors compared with classical numerical schemes. The obtained results indicate that the ANN-based approach can effectively approximate the stochastic system (2.2) under Lévy noise.

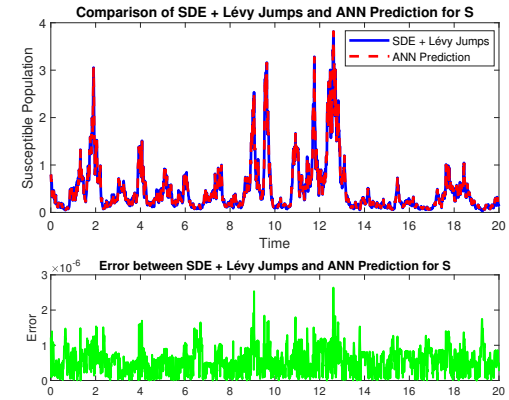

(a) Susceptible Class

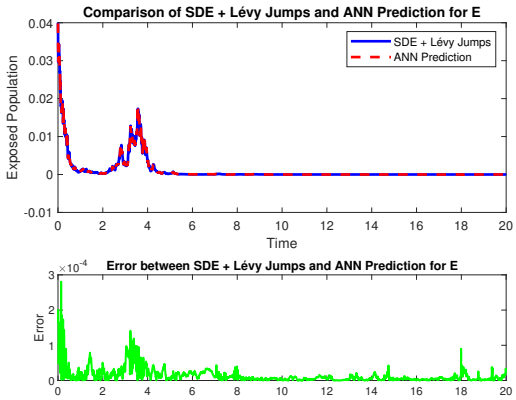

(b) Exposed Class

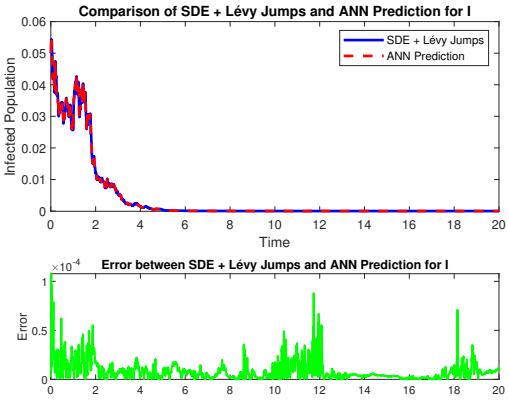

(c) Infected Class

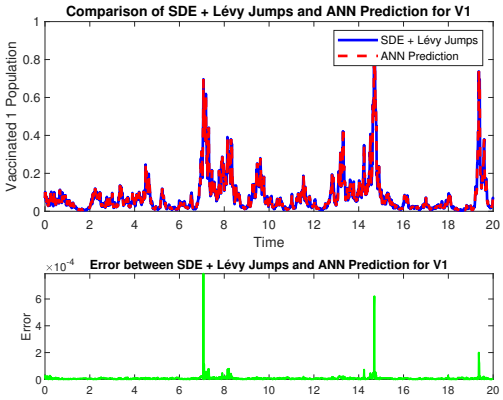

(d) First-dose vaccination

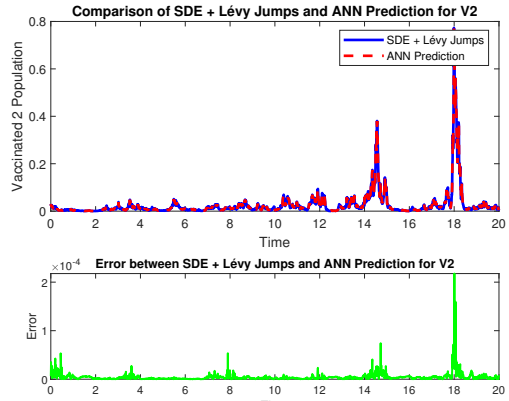

(e) Second-dose vaccination

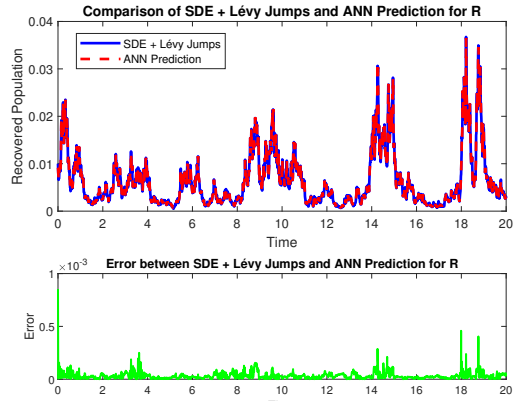

(f) Recovered Class

Figure 4. Comparison of ANN predictions with the proposed model (2.2) dynamics, together with the corresponding error plots.

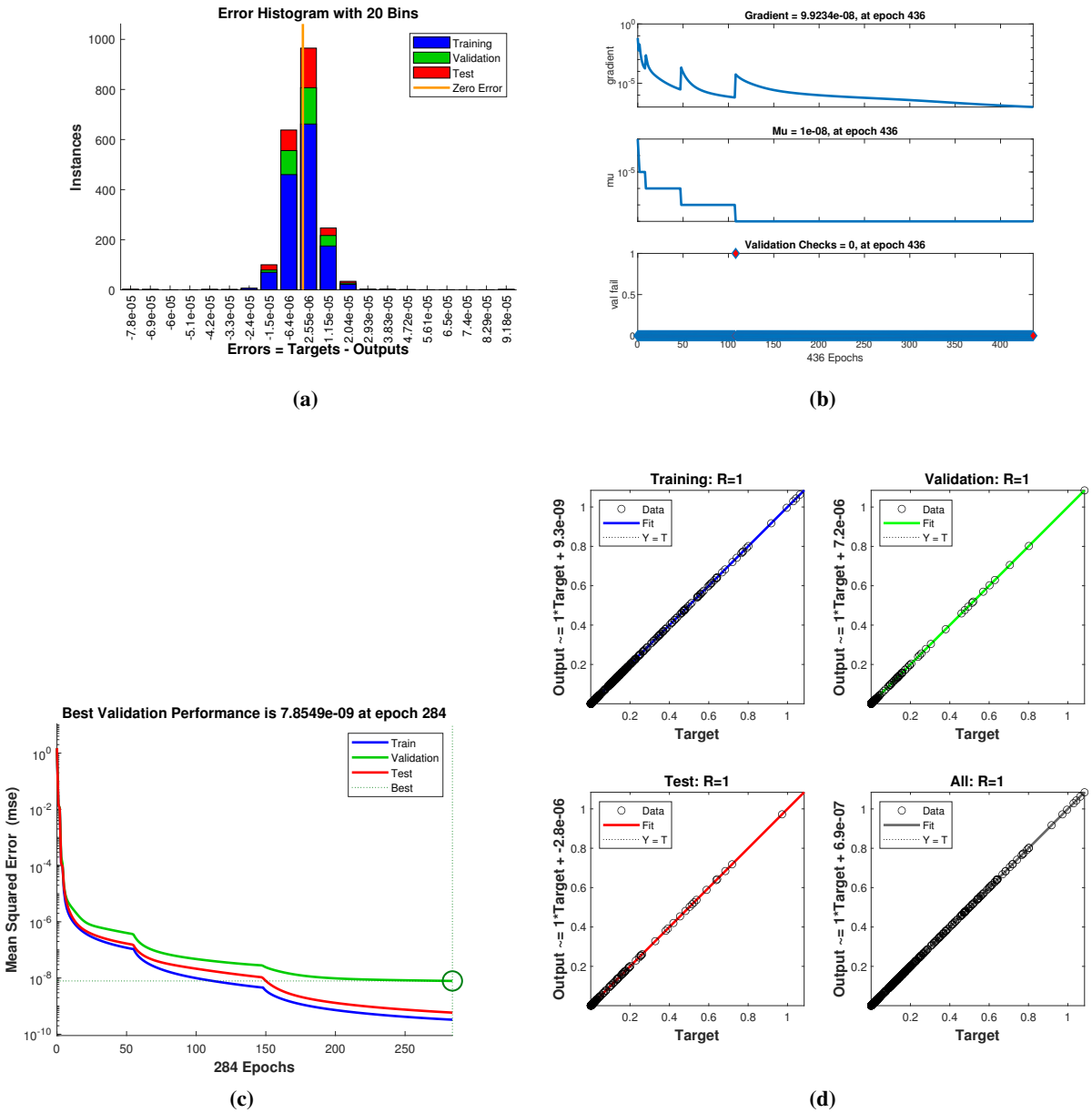

Figure 5. Panel (a) and (c) show the error histograms and the training, validation, and testing performance over epochs. Panels (b) and (d) display the corresponding output vs target plots for training, validation, and test data, illustrating the model's prediction accuracy at each stage.

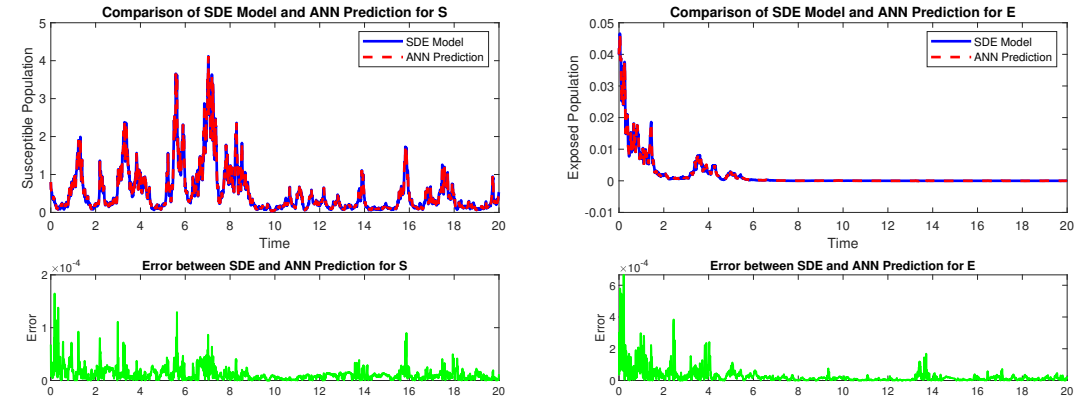

(a) Susceptible Class

(b) Exposed Class

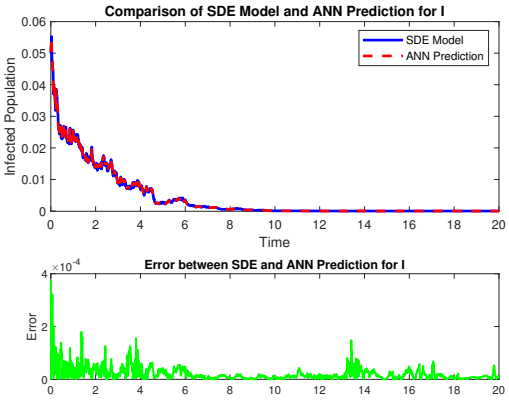

(c) Infected Class

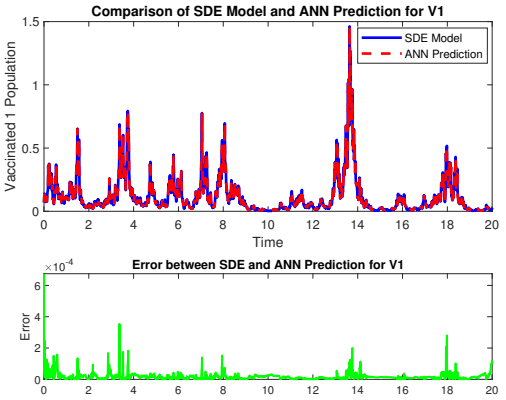

(d) First-dose vaccination

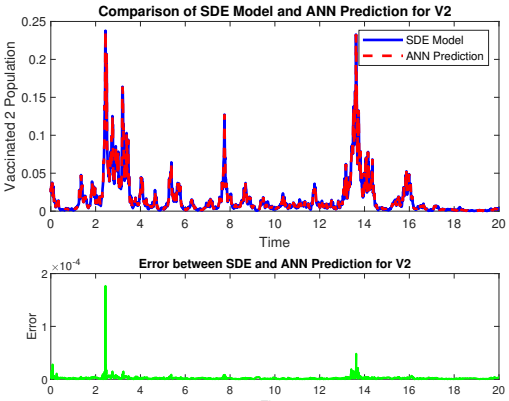

(e) Second-dose vaccination

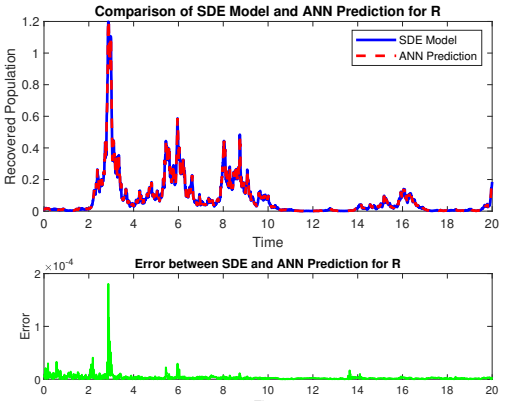

(f) Recovered Class

Figure 6. Comparison of ANN and Lévy noise on the solution trajectories of $\mathbb{S}(t), \mathbb{E}(t), \mathbb{I}(t), \mathbb{V}_1(t), \mathbb{V}_2(t), \mathbb{R}(t)$. Panels (a) and (b) show the comparison between the SDE model and ANN predictions for the $\mathbb{S}(t)$ and $\mathbb{E}(t)$ classes. Panels (c) and (d) display the comparison for the $\mathbb{I}(t)$ class and the $\mathbb{V}_1(t)$ classes. Panels (e) and (f) show the comparison for the $\mathbb{V}_2(t)$ and $\mathbb{R}(t)$ classes, along with the error plots.

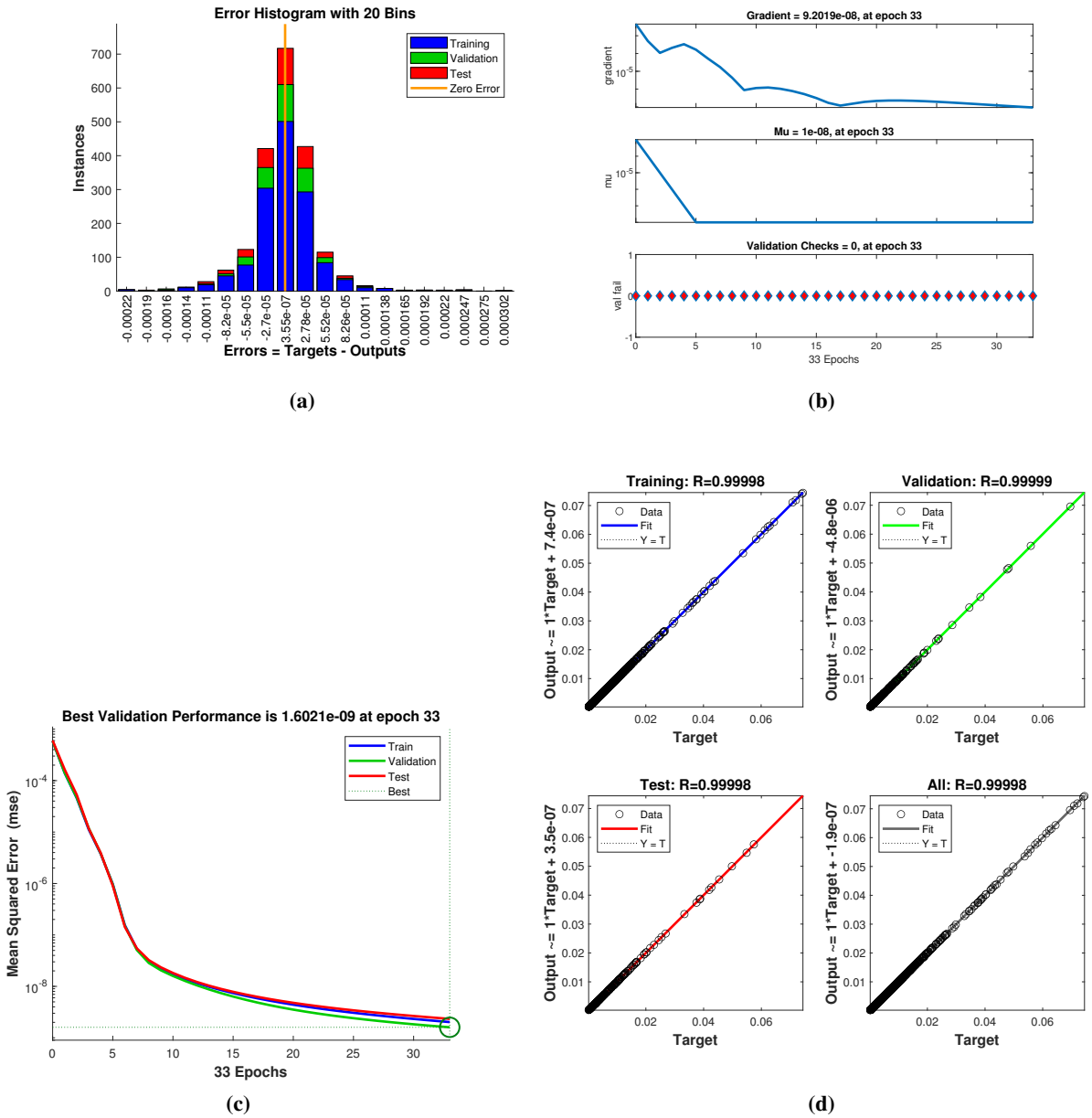

Figure 7. Shows an error histogram in (a) and a validation-based MSE curve in (c). Training behavior is shown in (b), while (d) compares predicted outputs against targets across data splits and reports the associated **R** statistics.

Table 2. Comparison of prediction errors between the proposed ANN-LMB framework and classical numerical methods.

Method	MSE	RMSE
Euler–Maruyama	0.0132	0.1150
Milstein Scheme	0.0094	0.0970
ANN-LMB	0.0031	0.0556

9. Conclusions

In this study, we developed a stochastic mathematical model to analyze the transmission dynamics of measles, incorporating Lévy noise to account for environmental disturbances. We established the existence and uniqueness of a global positive solution, ensuring the biological relevance of the model. A stochastic threshold was derived to determine whether the disease persists or extinguishes. When $\mathbf{R}_0 < 1$, the system is stochastically stable and leads to disease extinction. Conversely, when $\mathbf{R}_0^s > 1$, the disease persists, with the system oscillating around the endemic equilibrium of the deterministic model. Numerical simulations validated these theoretical findings, demonstrating that environmental noise can significantly influence disease dynamics, potentially driving the disease to extinction even when deterministic models predict persistence. Furthermore, we integrated ANNs to approximate the dynamics of the system with Lévy noise. The ANN was trained on time-series data and achieved remarkable accuracy in predicting transitions among the susceptible, exposed, infected, first-dose vaccinated, second-dose vaccinated, and recovered classes. The ANN model's ability to capture the stochastic dynamics of disease spread, despite the complexity introduced by Lévy jumps, highlights the power of neural networks in modeling complex epidemiological systems. The ANN successfully replicated the behavior of the proposed model with Lévy jumps, demonstrating both high accuracy and reliability across different stages of the disease progression. Future work can build on these findings by extending the model to include additional factors, such as waning immunity or public health campaigns, delayed trem, and by further refining its predictions through improved ANN architectures.

Use of Generative-AI tools declaration

The authors declare that they have not used Artificial Intelligence (AI) tools in the creation of this article.

Acknowledgement

This work was supported by the Research Startup Fund of Chengdu University of Technology (Grant No. 10912-KYQD2025-11350).

Conflict of Interest

The author declares that he has no conflict of interest.

References

1. *Measles*, World Health Organization, 2018. Available from: `https://www.who.int/zh/news-room/fact-sheets/detail/measles`.
2. C. J. Fraser-Bell, Global re-emergence of measles–2019 update, *Global Biosecur.*, 2019.
3. R. M. Anderson, R. M. May, *Infectious Diseases of Humans: Dynamics and Control*, Oxford: Oxford University Press, 1991.

4. M. Keeling, P. Rohani, *Modeling Infectious Diseases in Humans and Animals*, Princeton: Princeton University Press, 2008.
5. B. T. Grenfell, O. N. Bjornstad, J. Kappey, Traveling waves and spatial hierarchies in measles epidemics, *Nature*, **414** (2002), 716–723. https://doi.org/10.1038/414716a
6. N. C. Grassly, C. Fraser, Seasonal infectious disease epidemiology, *Proc. Biol. Soc.*, **273** (2006), 2541–2550. https://doi.org/10.1098/rspb.2006.3604
7. K. Xu, B. Gao, J. Li, Y. Xiang, L. Cao, M. Zhao, Clinical features, diagnosis, and management of COVID-19 vaccine-associated Vogt-Koyanagi-Harada disease, *Hum. Vacc. Immunother.*, **19** (2023), 2220630. https://doi.org/10.1080/21645515.2023.2220630
8. Y. Jia, B. Fu, L. Dong, M. Zhao, Sweet syndrome induced by SARS-CoV-2 vaccines: A systematic review of patient-report studies, *Hum. Vacc. Immunother.*, **19** (2023), 2217076. https://doi.org/10.1080/21645515.2023.2217076
9. X. Li, J. Xiang, F. Wu, M. Li, A dual ranking algorithm based on the multiplex network for heterogeneous complex disease analysis, *IEEE/ACM Trans. Comput. Biol. Bioinform.*, **19** (2022), 1993–2002. https://doi.org/10.1109/TCBB.2021.3059046
10. F. Brauer, C. Castillo-Chavez, *Mathematical Models in Epidemiology*, Berlin: Springer, 2008.
11. H. W. Hethcote, The mathematics of infectious diseases, *SIAM Rev.*, **42** (2000), 599–653. https://doi.org/10.1137/S0036144500371907
12. L. J. S. Allen, *Stochastic Population and Epidemic Models*, Berlin: Springer, 2017.
13. H. Andersson, T. Britton, *Stochastic Epidemic Models and Their Statistical Analysis*, Berlin: Springer, 2000.
14. A. Mozokhina, I. Popravka, M. Saade, V. Volpert, Epidemic model with time delays and fertility/mortality rates, *AIMS Math.*, **10** (2025), 25849–25878. https://doi/10.3934/math.20251143
15. S. Ouyang, G. Chen, Y. Xia, G. Shi, Y. Feng, Stochastic dynamics of influenza epidemic model with vaccination strategy, *AIMS Math.*, **10** (2025), 20412–20442. https://doi.org/10.3934/math.2025912
16. S. P. Rajasekar, M. Manju Priya, Dynamics on stationary distribution and probability density function of a $(2n+2)$ multi-strain stochastic epidemic model, In: *Biology and Sustainable Development Goals: Applications of Mathematical Methods*, Singapore: Springer Nature Singapore, 2025, 33–83.
17. S. P. Rajasekar, R. Ramesh, Y. Sabbar, Based on epidemiological parameter data, probe into a stochastically perturbed dominant variant of the COVID-19 pandemic model, *Gene*, **926** (2024), 148608. https://doi.org/10.1016/j.gene.2024.148608
18. A. Khan, A. Din, Stochastic analysis for measles transmission with Lévy noise: A case study, *AIMS Math.*, **8** (2023), 18696–18716. http://doi.org/10.3934/math.2023952
19. Weekly epidemiological record–Relevé épidémiologique hebdomadaire, *World Health Organization*, **15** (1940), 231.
20. O. J. Peter, M. M. Ojo, R. Viriyapong, F. A. Oguntolu, Mathematical model of measles transmission dynamics using real data from Nigeria, *J. Differ. Equ. Appl.*, **28** (2022), 753–770. https://doi.org/10.1080/10236198.2022.2079411

21. O. J. Peter, H. S. Panigoro, M. A. Ibrahim, O. M. Otunuga, T. A. Ayoola, A. O. Oladapo, Analysis and dynamics of measles with control strategies: A mathematical modeling approach, *Int. J. Dyn. Control*, **11** (2023), 2538–2552. https://doi.org/10.1007/s40435-022-01105-1
22. M. A. Ibrahim, A. Dénes, Stability and threshold dynamics in a seasonal mathematical model for measles outbreaks with double-dose vaccination, *Mathematics*, **11** (2023), 1791. https://doi.org/10.3390/math11081791
23. H. T. Alemneh, A. M. Belay, Modelling, analysis, and simulation of measles disease transmission dynamics, *Discrete Dyn. Nat. Soc.*, **2023** (2023), 9353540. https://doi.org/10.1155/2023/9353540
24. M. El Hajji, A. H. Albargi, A mathematical investigation of an SVEIR epidemic model for the measles transmission, *Math. Biosci. Eng.*, **19** (2022), 2853–2875. http://doi.org/10.3934/mbe.2022131
25. M. A. Kuddus, M. Mohiuddin, A. Rahman, Mathematical analysis of a measles transmission dynamics model in Bangladesh with double dose vaccination, *Sci. Rep.*, **11** (2021), 16571. https://doi.org/10.1038/s41598-021-95913-8
26. Z. Sabir, M. A. Z. Raja, A. S. Alnahdi, M. B. Jeelani, M. A. Abdelkawy, Numerical investigations of the nonlinear smoke model using the Gudermannian neural networks, *Math. Biosci. Eng.*, **19** (2022), 351–370. https://doi.org/10.3934/mbe.2022018
27. Z. Sabir, M. A. Z. Raja, J. L. Guirao, T. Saeed, Meyer wavelet neural networks to solve a novel design of fractional order pantograph Lane-Emden differential model, *Chaos Solitons Fract.*, **152** (2021), 111404. https://doi.org/10.1016/j.chaos.2021.111404
28. Z. Sabir, M. A. Z. Raja, M. Umar, M. Shoaib, D. Baleanu, FMNSICS: Fractional Meyer neuro-swarm intelligent computing solver for nonlinear fractional Lane-Emden systems, *Neural Comput. Appl.*, **34** (2022), 4193–4206. https://doi.org/10.1007/s00521-021-06452-2
29. J. Jin, W. Chen, A. Ouyang, F. Yu, H. Liu, A time-varying fuzzy parameter zeroing neural network for the synchronization of chaotic systems, *IEEE Trans. Emerg. Topics Comput. Intell.*, **8** (2024), 364–376. https://doi.org/10.1109/TETCI.2023.3301793
30. X. Hu, Y. Lu, G. Tian, P. Bing, B. Wang, B. He, Predicting herb-disease associations through graph convolutional network, *Curr. Bioinform.*, **18** (2023), 610–619. https://doi.org/10.2174/1574893618666230504143647
31. J. Xiang, J. Zhang, R. Zheng, X. Li, M. Li, NIDM: Network impulsive dynamics on multiplex biological network for disease-gene prediction, *Brief. Bioinform.*, **22** (2021), bbab080. https://doi.org/10.1093/bib/bbab080
32. K. Guedri, R. Zarin, M. Oreijah, S. K. Alharbi, H. A. E. W. Khalifa, Artificial neural network-driven modeling of Ebola transmission dynamics with delays and disability outcomes, *Comput. Biol. Chem.*, **115** (2025), 108350. https://doi.org/10.1016/j.compbiolchem.2025.108350
33. M. Farhan, Z. Ling, S. Ullah, M. Alsubhi, M. Asiri, M. B. Riaz, A novel physics-informed neural network approach to assess the impact of double-dose vaccination on measles transmission, *Eur. Phys. J. Plus*, **139** (2024), 1059. https://doi.org/10.1140/epjp/s13360-024-05838-0
34. H. Tahir, W. A. Khan, M. ur Rahman, Numerical investigation of a wireless sensor network epidemic model with α-stable noise: A case study, *AIMS Math.*, **10** (2025), 20312–20345. https://doi.org/10.3934/math.2025908

35. S. M. A. Shah, Y. Nie, A. Alkhazzan, C. Tunç, A stochastic hepatitis B model with media coverage and Lévy noise, *J. Taibah Univ. Sci.*, **18** (2024), 2414523. https://doi.org/10.1080/16583655.2024.2414523
36. A. Din, Y. Li, Lévy noise impact on a stochastic hepatitis B epidemic model under real statistical data and its fractal-fractional Atangana-Baleanu order model, *Phys. Scr.*, **96** (2021), 124008. https://doi.org/10.1088/1402-4896/ac1c1a
37. M. El Fatini, I. Sekkak, Lévy noise impact on a stochastic delayed epidemic model with Crowly-Martin incidence and crowding effect, *Phys. A*, **541** (2020), 123315. https://doi.org/10.1016/j.physa.2019.123315
38. X. B. Zhang, X. D. Wang, H. F. Huo, Extinction and stationary distribution of a stochastic SIRS epidemic model with standard incidence rate and partial immunity, *Phys. A*, **531** (2019), 121548. https://doi.org/10.1016/j.physa.2019.121548
39. M. Zahri, Multidimensional Milstein scheme for solving a stochastic model for prebiotic evolution, *J. Taibah Univ. Sci.*, **8** (2014), 186–198. https://doi.org/10.1016/j.jtusci.2013.12.002
40. D. Desta, A. Abebe, J. Brannan, Dynamical systems framework for modeling COVID-19 with Lévy noise, *Stoch. Dyn.*, **26** (2026), 2550040. https://doi.org/10.1142/S0219493725500406
41. X. N. Leng, T. Feng, X. Z. Meng, Stochastic inequalities and applications to dynamics analysis of a novel SIVS epidemic model with jumps, *J. Inequal. Appl.*, **2017** (2017), 138. https://doi.org/10.1186/s13660-017-1418-8
42. J. Danane, K. Allali, Z. Hammouch, K. S. Nisar, Mathematical analysis and simulation of a stochastic COVID-19 Lévy jump model with isolation strategy, *Results Phys.*, **23** (2021), 103994. https://doi.org/10.1016/j.rinp.2021.103994
43. X. Mao, F. Wei, T. Wiriyakraikul, Positivity preserving truncated Euler-Maruyama method for stochastic Lotka-Volterra competition model, *J. Comput. Appl. Math.*, **394** (2021), 113566. https://doi.org/10.1016/j.cam.2021.113566

AIMS Press